FACHHOCHSCHUL-MASTERSTUDIENGANG

AUTOMATISIERUNGSTECHNIK

THERMAL CHARACTERIZATION OF AN ELECTRIC POWER CONVERTER USING HARDWARE-IN-THE-LOOP SIMULATION

Research Paper

by

RAIMUND SCHRATTENECKER

January 2013

Assistance of the Research:

PROF. (FH) UNIV. DOZ. DIPL.-ING. DR. KARL KELLERMAYR

DR. MICHAEL STEURER

DR. JUAN ORDONEZ

Abstract

Currently a paradigm shift in the United States Navy is taking place. Today, most military vessels have seperated propulsion and supply energy systems. With the upcoming generation of ships, the so called All Electric Ship, this separation should be a thing of the past. To accomplish this substantial change further research efforts in different technological fields, are necessary.

This thesis is based on an actuall research project of the Center for Advanced Power Systems in Tallahassee, Florida. Funded by the US Navy's Electric Ship Research and Development Consortium, it shows the modeling and simulation of a cooling system that may be employed on future All Electric Ships.

The central issue addressed by this work is to show the modeling of the temperature behavior in the water cooling system of an All Electric Ship. For this reason a linear time-invariant third-order system is esablished. The resulting model is computed with Wolfram Mathematica and implemented and validated in a Matlab / Simulink simulation.

In the second part of the thesis the mathematical model is implemented into a hardware-in-the-loop simulation. For this reason it is extended by a real piece of hardware. In addition to the implementation of the model into a real time environment, the construction of the test bed is shown.

Contents

List of Figures

Part I

Motivation

1 Introduction

This master thesis is the result of an internship at the Center for Advanced Power Sytems (CAPS) in Tallahassee, Florida. CAPS is an important research partner for the United States Navy (USN) in developing a new type of naval vessel. This new ship type, more precisely the All-Electric Ship (AES), is part of an ambitious technology plan for the future United States of America (USA) Navy fleet. The key feature of an AES is the employment of an next generation integrated power system (NGIPS), which combines electric propulsion technology with other energy efficient power systems throughout the ship.
Today, most military vessels have seperated propulsion and supply energy systems. This seperation has several drawbacks, which can lead to a low overall system efficiency. The AES, however, has the potential to solve these problems, but further research efforts are still necessary. The current AES research puts the focus on:

- Power generation
- Power distribution
- Energy storage
- Heat transfer and thermal management
- Motors and actuators

The central issue addressed by this work is to show the modeling and simulation of the temperature behavior of the water cooling system of an AES. Also the validation of the simulation, based on an implementation into a hardware in the loop (HIL) scenario is shown.
The research is part of the Navy's mission to develop the next generation of destroyer battleships, the Zumwalt-class destroyer DDG-1000, which will be a class of most advanced AESs. In November 2001, the US Department of Defense announced, that the Zumwalt-class will replace the current Arleigh Burke-class

(DDG-51) as the Navy's multi mission destroyer.
Mathematical problems during the modeling process were solved by using Wolfram Mathematica. Matlab and Simulink were used for the basic modeling and simulation part. For the HIL simulation, RSCAD from RTDS Technologies was used which is a modeling software for the Real Time Digital Simulator (RTDS) from the CAPS.

2 The United States Navy's All-Electric Ship Concept

2.1 The United States Navy and the Electric Ship Research and Development Consortium

> "It follows then as certain as that night succeeds the day, that without a decisive naval force we can do nothing definitive, and with it, everything honorable and glorious." [3]

This personal quotation of President George Washington from 1781 has not lost any of its actuality during the last 230 years. With 287 deployable battle force ships and 318.406 personnel on active duty[1], the USN is today one of the largest naval forces in the world [4]. In order to maintain this status, the USN spends considerable efforts in the research of new innovative technologies for their fleet. One of these efforts was the foundation of the Electric Ship Research and Development Consortium (ESRDC) by the Office of Naval Research (ONR)[2] in 2002. Primary purpose of the ESRDC is the research and development of tools and technologies, which can be used to establish an electric naval force for the USN. For this reason the ESRDC combines programs and resources of leading power research institutions. Originally conceived with four universities, the consortium has expanded to a total of eight members till today. Member institutions include: The Florida State University, Massachusetts Institute of Technology, Mississippi State University, Naval Post Graduate School, Purdue University, United States Naval Academy, University of South Carolina, and the University of Texas at Austin. The consortium has five major thrusts:

[1] As at Oktober 2012.
[2] "The Office of Naval Research coordinates, executes, and promotes the science and technology programs of the United States Navy and Marine Corps" [5].

- Computational tools for early-stage ship design
- Ship electric power system
- Total ship system solution to thermal management
- Load management
- Next Generation Integrated Power System (NGIPS)

Through these thrusts, the Navy should get and maintain the scientific and technological base needed, to successfully actualize the idea of an AES [6]. The fact that the consortium was already able to contribute important accomplishments for this goal, shows that its work is a success. In the ten years of its existence, the ESRDC members were able to produce prototypes and simulation results, which helped the Navy to approve the funding for at least three major development programs with industry. Beside the apparent research reasons, the ESRDC also addresses the national shortage of electric power engineers by providing educational opportunities for students in state of the art experimental facilities. Since the consortium was established, more than 300 papers were presented and more than 50 students have received advanced degrees for research enabled through the ESRDC [7] [8].

2.2 The All-Electric Ship Concept

Since the technological capabilities and the geopolitical circumstances are in a steady progress, a variety of factors have an impact in the way the USN is designing and developing their future naval fleet. Volatile fuel costs and the reliability of the international oil supply for example, continues to be of concern to the US from a national security perspective. In addition, future implementation of new sensor and weaponry technologies, will require a change in upcoming shipboard energy utilization and thermal management systems [9].
To face these challanges, the USN is planing to complement their fleet by the new DDG-1000 Zumwalt class destroyer. Other than the current DDG-51 Arleigh Burke class destroyer, the Zumwalt class is equipped with an integrated power system (IPS). This difference represents a significant departure from traditional propulsion and energy systems, employed on earlier naval surface ships [10].

2.2.1 Conventional Ship Architecture

In this thesis the DDG-51 destroyer is used as an example for a ship with a conventional energy architecture. That means that the ship has seperated propulsion and service power systems. For the operation of a destroyer a huge amount of energy is needed. For this reason the DDG-51 employes in total seven prime movers, with a overall power of more than 80 MW. Four General Electric LM2500 gas turbines, which provide a overall power of $74,57$ MW, strictly dedicated to propulsion, as well as three Rolls Royce Allison 501-K34 which provide $7,5$ MW for the service electricity for the destroyer [11] [12]. Therefore 90 % of the available power capacity is exclusively used for propulsion. That allows the DDG-51 to reach a maximum speed of more than 30 knots, although the usual cruise speed rarely exceeds 20 knots. Because of the approximately cubic relationship between speed and required shaft power, about $\frac{2}{3}$ of the available power remains unused under the most common operating conditions. This circumstance, in combination with the poor part-load efficiency of gas turbines, leads to greater fuel consumption and therefore to a low overall efficiency.
However, the poor part-load efficiency is not the only downside of the conventional ship architecture. Another problem is that the prime movers which are dedicated for propulsion are mechanically connected to the propellers of the ship. This leads to an additional mechanical effort, because large gearboxes are needed, which convert the revolution speed of the gas turbines to the much lower rotation speed of the propellers. Using the example of the DDG-51 destroyer, two additional gearboxes are needed to connect the four gas turbines to the two propellers of the ship (see figure 2.1).

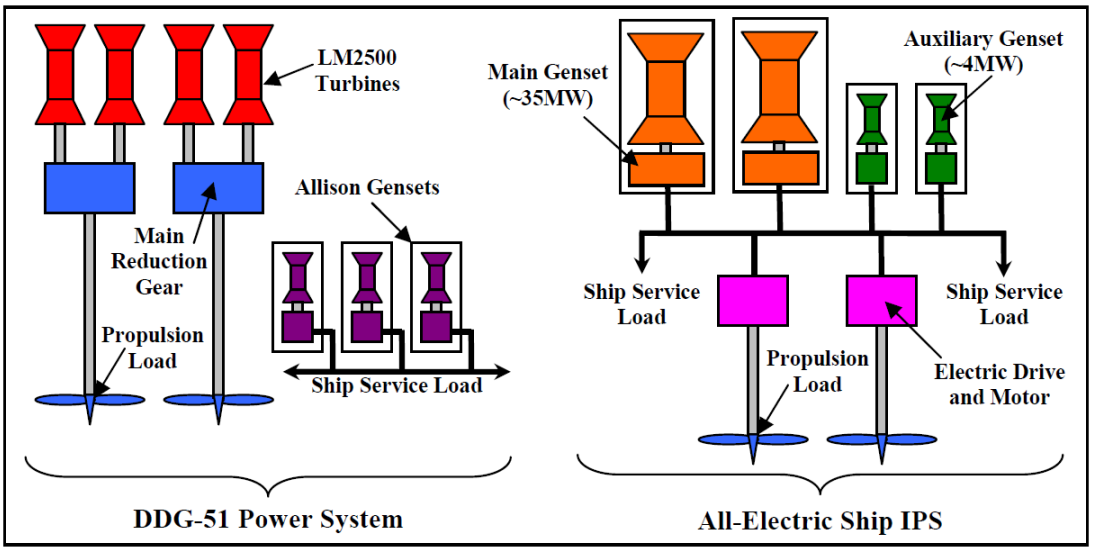

Figure 2.1: Comparison of the DDG-51 power system and the DDG-1000 IPS system [10]

Another drawback of mechanical propulsion systems is that most prime movers are not reversible. That means that special reversing gearboxes or variable-pitch propellers are needed to back the ship. This generally has a negative impact on the costs, complexity and fuel consumption of the propulsion system. Furthermore, can waves and other environmental factors induce propulsion transients to the prime movers over the mechanical connection to the propeller. This leads to increased fuel consumption and higher maintenance costs [11].
Because of these disadvantages, the USN is interested in the development of new, innovative propulsion and energy systems which are able to resolve the current problems and are all set to face the technological challanges of the upcoming years as well.

2.2.2 Integrated Power System Architecture for the Future All-Electric Ship

As mentioned above, the next generation of naval surface ships will be equiped with an IPS. The major idea behind the IPS approach is that all the generated power from the prime movers is converted to electricity. On this way all the available energy can be intelligently distributed throughout the ship and is not longer restricted to a special application. A basic requirement for the implementation of such an IPS is that the vast majority of the hydraulic, pneumatic and mechanical systems on the ship have to be replaced by electrical one. That is also true for

the ships propulsion system, where low-speed electromagnetic motors are directly connected to the propeller shaft. On this way most of the problems occurring because of the mechanical connection between prime movers and propeller can be avoided. Reduction and reversion gearboxes are not longer necessary. Compared to conventional energy systems of current ships, the IPS approach enables a considerably increase of flexibility which leads to a lower total number of needed prime movers. The DDG-1000 destroyer for example, will be powered by only four gas turbines with a total power of $80 - 90\,\mathrm{MW}$ (see figure 2.1). At the same time there will be more power available for other systems than propulsion. That is especially important considering the future development in the sensor and electric weapon area [11]. An additional advantage of the IPS is that supplementary energy sources can feed directly into the electrical grid. This allows for example the deployment of heat recovery units and brake power recovery systems, while energy storage units, like electric batteries or flywheels provide the possibility to store every overproduction of electricity for later utilization.
All in all the IPS approach provides numerous benefits, including:

- decreased maintenance requirements because of similarities of ship systems.
- increased ship survivability during combat missions due to reconfigurability and system redundancies.
- system adaptability which allows the implementation of future high-energy sensor and weapon systems.
- flexibility in the situational power distribution which allows systems to operate at their optimum operating point.
- increased efficiency, reliability and reduced operational costs and repair downtimes.
- higher automation potential allows a reduced number of crew members [11] [13].

2.3 All-Electric Ship Research Topics and Problem Outline

However, before the AES concept can unfold its full potential, numerous technical challenges have to be overcome. One issue for example, is the reliability of the

electrical distribution system. Propulsion and weapon systems that were self sufficient with the traditional ship architecture depent now on a robust and resilient electrical feed. Beyond the bare survivability, the electrical grid must also remain stable enough to support sensitiv electronic loads. This challange is especially hard to meet, considering the specific electrical characteristic of a ship. In case of the DDG-1000 for example, the total propulsion power represents approximately $86,5\,\%$ of the total installed electrical power on the ship. A propulsion motor trip during full load, would induce transients hardly seen in a terrestrial grid [11].
Advanced grid management concepts, hold the potential to fulfill these needs also during extrem situations. Nevertheless, the best grid managment concept can not work without the proper working conditions. To meet the basic requirements for a robust electrical grid, a resilient, reliable and effective cooling system is indispensable in respect of maintaining survivability. Increased temperature creates frailty in conductors and interconnects or can cause rapid aging and deterioration of insulators. That is why the Department of Defense stated in 2005 that heat is the second largest cause of failure in electronic equipment [14]. Because the AES will provide more power for other systems but propulsion, additional electrical systems are capable of being deployed. High energy sensor and weapon systems as well as other high power electronic equipment have the potential to boost the requirement for cooling capacity by as much as $500 - 700\,\%$ compared to conventional ships. To meet the requirement of dramatic increased cooling capacity, while concurrently increasing survivability and flexibility is one of the major challanges in the design of future AESs [10].
Faced with this entire new concept of ship energy architecture, high uncertainty of the employed systems and other technical challanges the USN has invested substantially in the inprovement of their modeling and simulation capabilities. With the proper validation, simulations can be used as a useful tool in the design process of advanced shipboard technologies. The Navys incentive for this investment is the identification of problems, prospects and solutions prior to construction. With this kind of computational simulation, novel ship systems and advanced shipboard technologies can be developed faster and at a fraction of the costs than it would be possible with a physical mockup [11]. Because of these obvious advantages of modeling and simulation tools, it seems reasonable to employ them also for the development of a proper cooling strategy on the AES. In fact, due to their flexibility, computational simulations are a perfect tool to design the dynamically reconfigurable thermal management systems of the future AES. With the help of suitable simulations the time and cost effort for physical

mockups can be reduced to a minimum.
Of course, also the simulation of a technical system can not be done without a considerable amount of effort. The precondition for a useful and reliable simulation is a accurate model of the physical system. The fastest computers and the best simulations are useless if the underlying model does not describe the real conditions.

2.4 Detailed Goal of the Thesis and Related Work

The central issue addressed by this work is to show the modeling and simulation of the temperature behavior in the water cooling system of an AES. Further, the thesis shows a way to validate the simulation by implementing it into a HIL scenario. The mathematical problems during the modeling process were solved by using Wolfram Mathematica. MathWorks Matlab and Simulink were used for the basic simulation. The HIL simulation was done in a real time environment by using the RTDS located in the CAPS in Tallahassee, Florida.
The AES topic was already addressed by numerous research papers and theses. However, most of the realized research dealt with the wide-ranging field of energy distribution. Compared to this field the AES's cooling system is rather less investigated. In 2008, Heriberto Cortes [15] explored the thermal response of ship propulsion systems to load variations. In the same work he took a closer look into the recovery of waste heat from hot exhaust. In 2007, Patrick Paullus [10] presented a work dealing with the creation of specific thermal/fluid component models, which could be used for the simulation of a freshwater chilling loop on a DDG-51 class destroyer. Research efforts at the University of Texas in Austin, focused on the development of dynamic models of components that can be used to simulate the thermal architecture of future AESs. This research has resulted in the development of a thermal management tool, known as the Dynamic Thermal Modeling and Simulation Framework. Exemplary for this effort is the work of Michael Pierce in 2009 [13]. Around the same time Omar Faruque and Venkata Dinavahi from the University of Alberta and Michael Sloderbeck and Michael Steurer from the Florida State University did a thermo-electric co-simulation of an all-electric ship type notional system using two geographically distributed heterogeneous real-time simulators [16].

Part II

System Analysis and Modeling

3 Energy Distribution System

3.1 Medium Voltage Direct Current System

One of the characteristics of the IPS is that the entire electrical energy in the system is generated with only a small number of power generation modules (PGM). The architecture of the PGMs is not of particular importance for the functionality of the IPS. Gas turbines can act as prime movers as well as fuel cells or diesel engines. From these central points of energy production, the electricity is distributed to a multitude of different loads all over the ship [17].
For this energy distribution, future ships will employ a medium voltage direct current system (MVDC). The distributed power will employ voltages in the range of $\pm 3000\,\mathrm{V}$ to $\pm 10000\,\mathrm{V}$. The deployment of such a system brings many beneficial effects compared to the use of a conventional medium voltage alternating current (MVAC) system. One of the advantages is that the prime movers are not longer coupled to the frequency of the bus. This allows the optimization of the generator for each type of prime mover, without the need of additional speed reduction or increasing gears. Furthermore the number of generator poles is not longer a question of substance. Due to the lack of skin effect and reactive power, the MVDC system has even the potential to reduce cable weight. Also the paralleling of generators is easier with a MVDC system compared to a conventional MVAC system, because it only requires voltage matching instead of time critical phase matching. Because of the wider spectrum of operating frequencies, the MVDC system has also the capability to reduce the acoustic signature of the ship. An advantage which can help to remain undiscovered during mission [17].
Of course the electricity distributed in the MVDC grid can not be directly used to energize any equipment. It first has to be converted to a voltage suitable for the particular load. For this purpose the USN will employ power conversion modules (PCM) on their ships. Figure 3.1 shows a notional architecture for such a PCM. With these modules the voltage from the MVDC grid can be converted to 750-800 V DC power, 650 V DC power, another user-needed DC voltage, or 450 V AC power with a frequency of 60 Hz. A good PCM architecture should be open and

modular to match zonal energy demands and to ensure a high degree of flexibility. Therefore a PCM is composed of a number of ship service converter modules (SSCM) for DC loads and a number of ship service inverter modules (SSIM) for AC loads. These modules can be paralleled to provide redundancy and the required power rating. The optimal power ratings for the individual SSCMs and SSIMs requires further studies but the authors of the NGIPS technology development roadmap [17] assume that ratings on the order of 35 kW, 100 kW, and 300 kW would provide a considerable amount of design flexibility to optimize reliability, cost, and efficiency.

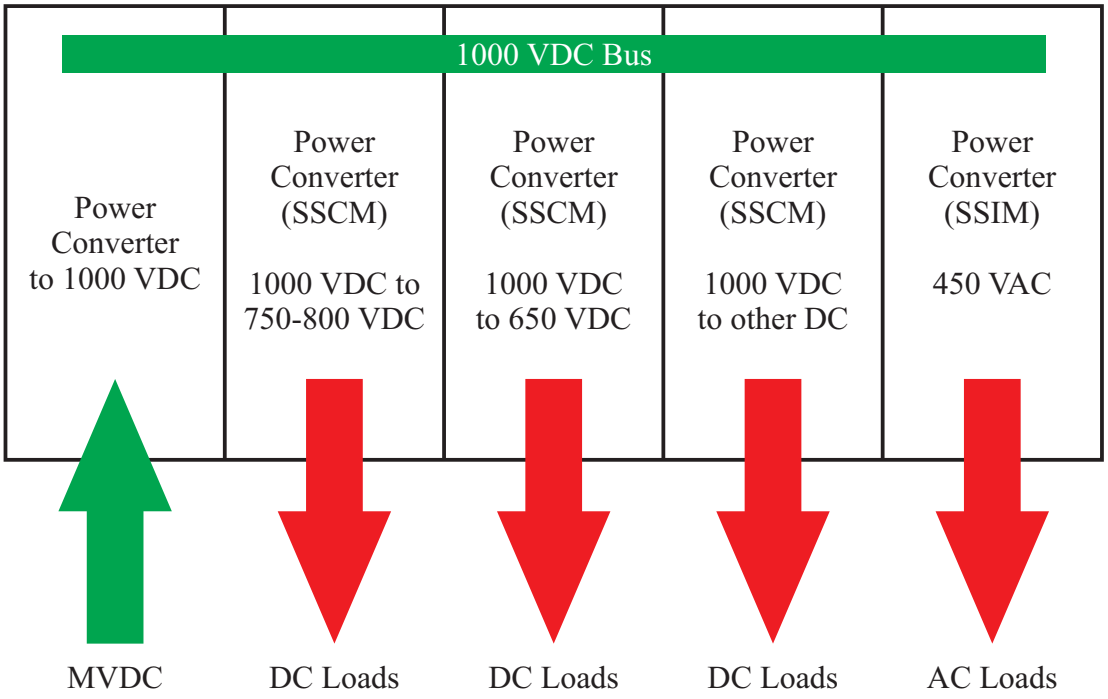

Figure 3.1: Structure of a power conversion module [17, modified].

3.2 Rectifier and Converter

Chapter 3.1 shows that the future AES will rely on a high number of rectifiers, converters and other high power electronic devices to distribute the electrical energy on the ship. These devices on the other hand employ a multitude of electronic components such as thyristors, MOSFETs and IGBTs which can be grouped under the umbrella term controllable switches. A controllable switch has the following ideal characteristics:

- Block forward and reverse voltages of any order with zero current flow in

off state.

- Conduct currents of any order with zero voltage drop in on state.
- Switch instantaneously between on and off state or vice versa when triggered.
- Demand negligible power from control source to trigger the switch.

Of course, real devices do not show these ideal characteristics. That is the reason why they dissipate power during operation. If this dissipated power exceeds a crucial limit value, the devices can fail and destroy themselves and also may damage other system components. In order to avoid these damages, it is necessary to conduct the emerging heat away from the switches and release the energy into the environment where it can not lead to further harm [18].

4 Thermal Management System

4.1 The First Law of Thermodynamics

The AES cooling system is based on heat transfer processes. To understand these processes, it is necessary to understand the relationships, but also the differences between the subjects of heat transfer and thermodynamics.
Although thermodynamics is concerned with heat interaction, it considers neither the mechanisms of heat exchange nor the methods that exist for calculating the rate of this exchange. The major difference between heat transfer and thermodynamics is, that thermodynamics deals with equilibrium states of matter, whereas heat transfer is inherently a nonequilibrium process. For heat transfer to occur, there must be a temperature gradient and therefore, thermodynamic nonequilibrium. The discipline of heat transfer quantifies the rate at which heat transfer occurs in terms of degree of thermal nonequilibrium, a quantification that inherently cannot be done with thermodynamic laws [19].
However, the subjects of thermodynamics and heat transfer are of course highly complementary. A possible point of view is to see the subject of heat transfer as an extension of thermodynamics. Especially the first law of thermodynamics, often called *the law of conservation of energy*, provides a useful, often essential, tool for many heat transfer problems. Basically, the first law of thermodynamics

is a statement that the total energy of a system remains constant as long as no energy crosses its boundaries. For a closed system there are only two ways how energy can cross the borders: heat transfer through the boundaries and work done by or on the system. This leads to the following equation of the first law for a closed system:

$$\Delta E_{st}^{tot} = Q - W \tag{4.1}$$

ΔE_{st}^{tot} is the change of total energy stored inside the system, Q is the heat transferred into the system, and W is the work done by the system [19].
Furthermore, the first law can also be applied to a control volume that is bounded by a control surface through which mass may pass. Mass entering or leaving the control volume carries energy with it. This process, called energy advection, adds a third way how energy can be introduced into the control volume. With this knowledge it can be said that there are three ways for energy to enter or leave the control volume: heat transfer through the boundaries, work done on or by the control volume and energy advection [19]. A true statement for the first law of thermodynamics can be very simply stated as follows:

> *"The increase in the amount of energy stored in a control volume must equal the amount of energy that enters the control volume, minus the amount of energy that leaves the control volume [19]."*

As shown in equation 4.1, the first law of thermodynamics addresses total energy. Total energy consists of kinetic, potential and internal energies. Together, kinetic and potential energies are usually known as mechanical energy. Internal energy can be further subdivided into thermal, chemical, nuclear and other kinds of energies. This thesis will focus attention on the thermal and mechanical forms of energy. Important for considerations on these energies is the knowledge, that the sum of mechanical and thermal energy is not conserved. The reason is, that energy conversion between different forms of energy and thermal energy can occur. A chemical reaction inside the control volume, for example, can transfer chemical into thermal energy. Because of this, a possible perception is to think of energy conversion as resulting in thermal energy generation. This generation can either be positive or negative [19]. If the inflow and generation of thermal and mechanical energy equals the outflow, a steady state condition must prevail inside the control volume. That means that the amount of thermal and mechanical

energy stored in the control volume must be constant. With this knowledge the above mentioned statement can be adapted to be well suited for heat transfer analysis:

> *"The increase in the amount of thermal and mechanical energy stored in the control volume must equal the amount of thermal and mechanical energy that enters the control volume, minus the amount of thermal and mechanical energy that leaves the control volume, plus the amount of thermal energy that is generated within the control volume [19]."*

This statement can also be written as:

$$\Delta E_{st} = E_{in} - E_{out} + E_g \tag{4.2}$$

In contrast to E^{tot} for total energy from equation 4.1, E stands for the sum of thermal and mechanical energy. The subscript st shows that it is a stored energy and Δ refers to the change over the time interval Δt. The subscripts in and out refer to energy entering and leaving the control volume whereas E_g stands for the generated thermal energy.
These statements are true over a time interval Δt, where all the energy terms are measured in joules. Of course, the first law of thermodynamics must be satisfied in every instant of time. Therefore it is possible to formulate the law on a rate basis. At any instant, there must be a balance between all energy rates:

$$\dot{E}_{st} \equiv \frac{dE_{st}}{dt} = \dot{E}_{in} - \dot{E}_{out} + \dot{E}_g \tag{4.3}$$

In this case all energy rates are measured in joules per second [19].
Equations 4.2 and 4.3 are often essential for solving heat transfer problems. The first step for applying the first law to a heat transfer problem is to identify an appropriate control volume and its control surface. The second step is to make a decision whether to perform the analysis for a time interval Δt (equation 4.2) or on a rate basis (equation 4.3). This decision depends mainly on the goal of the research and the way in which information about the system is available. The final step is to identify all relevant energy terms in the system. The stored energy E_{st}, the conversion from different forms of energy to thermal energy E_g, and finally the thermal and mechanical energy transport across the control surface E_{in} and

E_{out}[19].
In the statement of the first law (equation 4.1) the total energy, E^{tot}, includes kinetic energy (KE), potential energy (PE), and internal energy (U). KE is defined as:

$$KE = {}^1\!/_2 mV^2$$

where m is mass and V is velocity. PE is defined as:

$$PE = mgz$$

where g is the gravitational acceleration and z is the vertical coordinate. The internal energy consists of a sensible component, a latent component, a chemical component and a nuclear component. Crucial for the study of heat transfer are mainly the sensible (U_{sens}) and latent (U_{lat}) components. U_{sens} accounts for the translational, rotational, and vibrational motion of the atoms comprising the matter. U_{lat} relates to intermolecular forces which are influencing phase change between solid, liquid and vapor states. Together they are referred to as thermal energy, U_t. The sensible energy is mainly related to temperature and pressure, whereas the latent energy is the component associated with changes in phase. The latent energy increases if the medium changes from solid to liquid or from liquid to vapor and decreases from vapor to liquid and from liquid to solid. If no change in phase happens no change in latent energy occurs. Based on this, E_{st} can be written as:

$$E_{st} = KE + PE + U_t$$

Where $U_t = U_{sens} + U_{lat}$. If no phase change occurs, U_t reduces to U_{sens}. In many heat transfer problems KE and PE can further be neglected. That leads to, $E_{st} = U_{sens}$ [19].
The generated energy term covers every conversions from other form of internal energy to thermal energy. These conversions are volumetric phenomena, that are generally proportional to the magnitude of the volume of the control volume. A source for thermal energy, for example, could be the conversion from electrical energy to heat when a current is passed through a conductor. Depending on the resistance of the conductor, electrical energy is dissipated at a rate RI^2, which equals to the rate at which thermal energy is released within the control volume. For the study of heat transfer, every conversion from electrical, chemical, nuclear or electromagnetic effects, are treated either as sources or as sinks of thermal

energy and hence are included in the generation terms of equations 4.2 and 4.3 [19].

The in- and outflow terms are surface phenomena that are generally proportional to the surface area. They include heat transfer and work interactions occurring at the system boundaries. Also energy transfer through advection is considered in the in- and outflow terms. For instance, if the mass flow through the system boundaries is $\dot{m}$, the energy exchange from, or into, the system is $\dot{m}(u_t + {}^1\!/_2 V^2 + gz)$, where u_t is the thermal energy by unit mass.

If the first law is applied to a control volume with fluid crossing the system boundaries, the work term can be divided into two separate components. One component, termed flow work, describes the work which is done by pressure forces, moving fluid through the system boundaries. For a unit mass, this work is equivalent to the product of pressure and specific volume of the fluid (pv). The second component, $\dot{W}$, describes every other work which is done by the system. If the system is under steady state conditions, which means $\frac{dE_{st}}{dt} = 0$, and there is no thermal energy generation within the boundaries, equation 4.3 simplifies to the *steady flow energy equation* (see also figure 4.1):

$$\dot{m}(u_t + pv + {}^1\!/_2 V^2 + gz)_{in} - \dot{m}(u_t + pv + {}^1\!/_2 V^2 + gz)_{out} + q - \dot{W} = 0 \qquad (4.4)$$

The terms within the brackets constitute the energy for a unit mass of fluid at the in- and outflow locations of the system. Multiplied by the mass flow rate $\dot{m}$, they yield the rate at which the corresponding type of energy enters or leaves the control volume. Another expression for the sum of thermal energy and flow work per unit mass is enthalpy per unit mass, $i = u_t + pv$ [19].

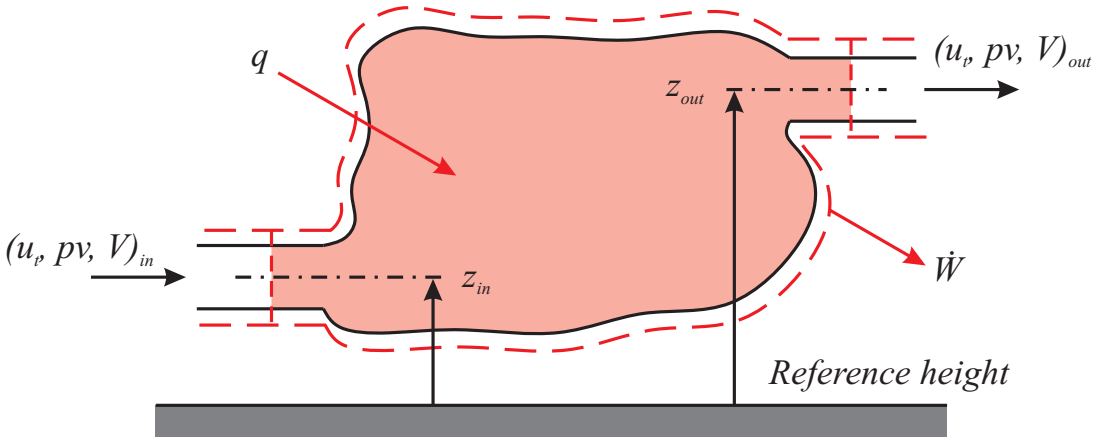

Figure 4.1: Conservation of energy for a steady flow, open system [19, modified].

However, in numerous technical applications, equation 4.4 can further be simplified. For systems without a phase change between in- and outlet (no latent energy change), the thermal energy, u_t reduces to its sensible component. If the fluid is approximated as an ideal gas with constant specific heats, the difference between enthalpies per unit mass can be expressed as $(i_{in} - i_{out}) = c_p(T_{in} - T_{out})$, where c_p is the specific heat at constant pressure and T_{in} and T_{out} are the in- and outlet temperatures of the system. If the fluid is an incompressible liquid, its specific heats at constant volume and pressure are equal. The change in sensible energy in equation 4.4, can therefore be written as $(u_{sens,in} - u_{sens,out}) = c_p(T_{in} - T_{out})$. Unless the pressure drop inside the control volume is extremely large, the difference between the in- and outlet flow work $(pv)_{in} - (pv)_{out}$, is negligible.
To summarize, for a system with an, incompressible liquid, negligible potential and kinetic energy changes, and negligible work, equation 4.4 can be written as the *simplified steady state flow thermal energy equation* [19]:

$$q = \dot{m}c_p(T_{in} - T_{out}) \tag{4.5}$$

4.2 Heat Exchanger

As mentioned in chapter 4.3, the AES employs a heat exchanger to transfer thermal energy between two cooling cycles. Heat exchangers are used to exchange heat between two fluids that are seperated by a solid wall and are at different temperatures. They can be found in many engineering applications like space heating, air-conditioning, power production, waste heat recovery and chemical

processing. Heat exchangers are classified according to their type of construction and flow arrangement. The most common types are: parallel-flow, conterflow, cross-flow and shell and tube heat exchanger.
In the most basic type of heat exchanger, the parallel-flow and counterflow devices, the fluids move in the same or opposite directions in a double pipe construction. In the parallel-flow type, shown in figure 4.2*a*, the fluids enter at the same side, move into the same direction and leave the exchanger at the same end. In the counterflow arrangement of figure 4.2*b*, the fluids enter at opposite ends, flow into opposite directions and leave the heat exchanger at opposite outlets [19]. For this thesis, knowledge about other types of heat exchangers is not necessary. Detailed information about other types can be found in appropriate specialist literature, like [19] or [20].

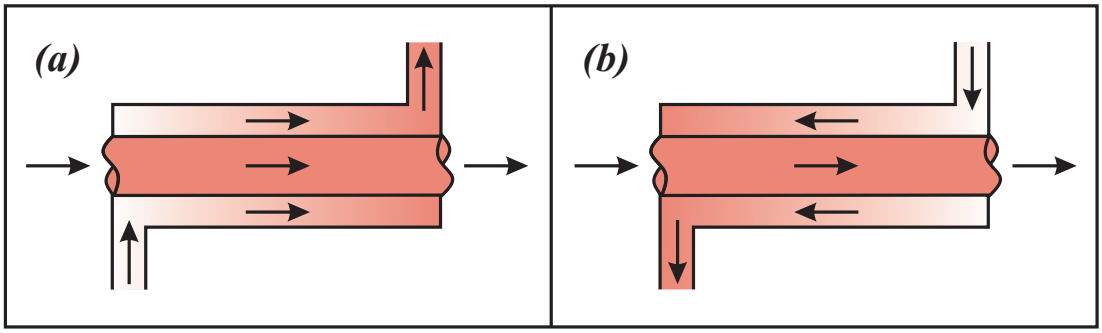

Figure 4.2: Concentric tube heat exchagner: ***(a)*** parallel flow, ***(b)*** counterflow [19, modified].

4.2.1 Energy Balance

To predict the performance of a heat exchanger, it is necessary to relate the total heat transfer rate to characteristics such as the in- and outlet fluid temperature, the total surface area for heat transfer and the overall heat transfer coefficient. This relationship can be obtained by applying overall energy balances to the hot and cold fluids, as shown in figure 4.3 [19].

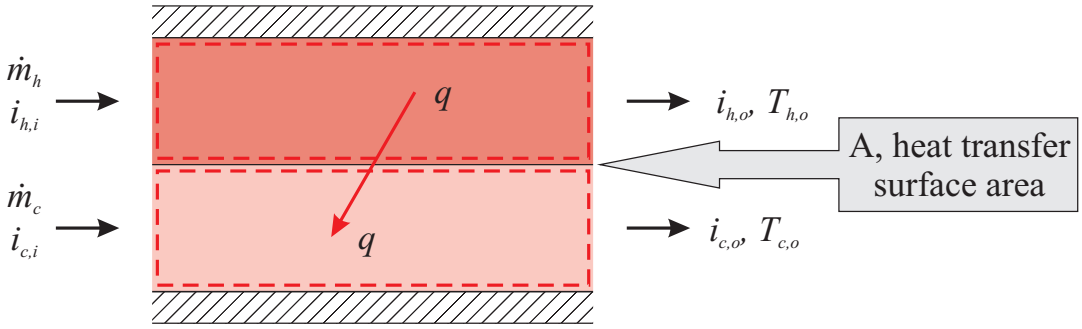

Figure 4.3: Overall energy balance for a two fluid heat exchanger [19, modified].

Provided that there is negligible heat transfer between apparatus and surroundings and negligible kinetic and potential energy changes, application of the steady flow energy equation 4.4 gives the total rate of heat transfer between the hot and cold fluid (q):

$$q = \dot{m}_h(i_{h,i} - i_{h,o}) \tag{4.6}$$

and

$$q = \dot{m}_c(i_{c,o} - i_{c,i}) \tag{4.7}$$

where i is the fluid enthalpy and the subscripts h and c refer to the hot and cold fluids, whereas i and o refer to the in- and outlet conditions. With regard to equation 4.5, further simplifications are possible. Assuming that no phase change (and therefore no change in latent energy) occurs, and constant specific heats are given, equations 4.6 and 4.7 can be written as:

$$q = \dot{m}_h c_{p,h}(T_{h,i} - T_{h,o}) \tag{4.8}$$

and

$$q = \dot{m}_c c_{p,c}(T_{c,o} - T_{c,i}) \tag{4.9}$$

The temperatures within the brackets stand for the mean fluid temperature at the designated locations. Equations 4.6 to 4.9 are neither coupled to a particular type of heat exchanger nor to a specific flow arrangement [19].

4.2.2 Effectiveness

The heat-exchanger effectiveness (ε) is the ratio between the actual rate of heat transfer (q), and the maximum possible heat transfer rate if the heat transfer area of the exchanger would be infinite q_{max}.

$$\varepsilon = \frac{q}{q_{max}} \tag{4.10}$$

q_{max} is a hypothetical value that could in principle be achivied in a counterflow heat exchanger (figure 4.4) of infinite length. In such a device, one of the fluids would experience the highest possible temperature change $T_{h,i} - T_{c,i}$. Refering to equations 4.8 and 4.9, $|\Delta T_c| > |\Delta T_h|$ would be true for every situation in which $(\dot{m}_c c_{p,c}) < (\dot{m}_h c_{p,h})$. That means that the cold fluid would experience the larger temperature change, and because of the infinte length of the exchanger it would be heated to the inlet temperature of the hot fluid ($T_{c,o} = T_{h,i}$).

$$\dot{m}_c c_{p,c} < \dot{m}_h c_{p,h} : \qquad q_{max} = \dot{m}_c c_{p,c}(T_{h,i} - T_{c,i})$$

For the opposite case in which $(\dot{m}_h c_{p,h}) < (\dot{m}_c c_{p,c})$, the hot fluid would experience the larger temperature change. In this case the hot fluid would be cooled to the inlet temerature of the cold fluid ($T_{h,o} = T_{c,i}$).

$$\dot{m}_h c_{p,h} < \dot{m}_c c_{p,c} : \qquad q_{max} = \dot{m}_h c_{p,h}(T_{h,i} - T_{c,i})$$

These results lead to the general expression:

$$q_{max} = \min\left\{(\dot{m}_h c_{p,h}), (\dot{m}_c c_{p,c})\right\}(T_{h,i} - T_{c,i}) \tag{4.11}$$

Applying equations 4.8, 4.9 and 4.11 to equation 4.10, it follows that:

$$\varepsilon = \frac{\dot{m}_h c_{p,h}(T_{h,i} - T_{h,o})}{min\left\{(\dot{m}_h c_{p,h}), (\dot{m}_c c_{p,c})\right\}(T_{h,i} - T_{c,i})} \tag{4.12}$$

or

$$\varepsilon = \frac{\dot{m}_c c_{p,c}(T_{c,o} - T_{c,i})}{min\left\{(\dot{m}_h c_{p,h}), (\dot{m}_c c_{p,c})\right\}(T_{h,i} - T_{c,i})} \tag{4.13}$$

By definition the effectiveness is dimensionless and has to be in the range $0 \leq \varepsilon \leq 1$ [19].

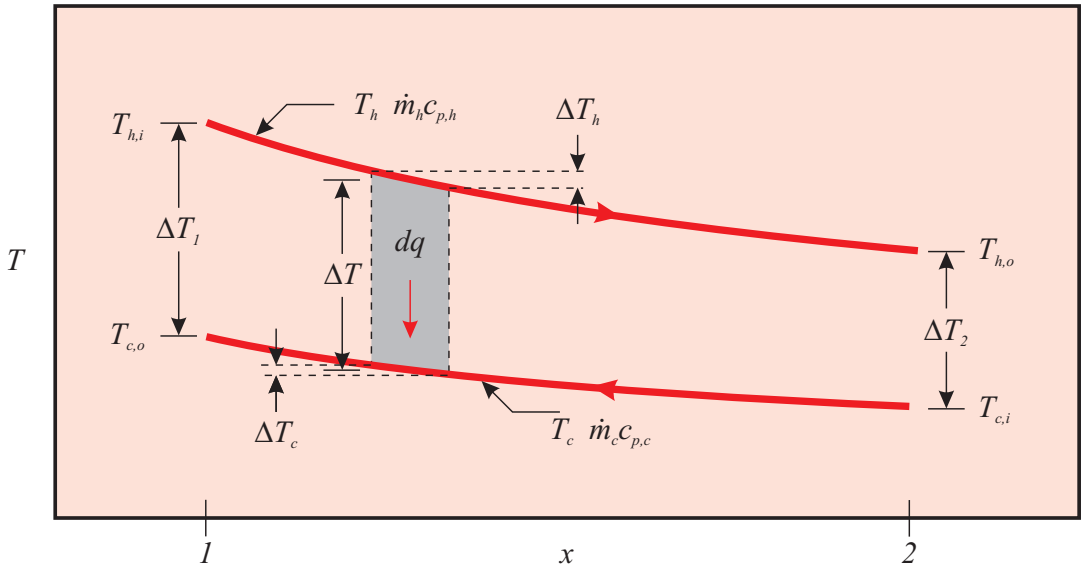

Figure 4.4: Temperature distributions for a counterflow heat exchanger [19, modified].

4.3 AES Cooling System

Chapter 3.2 shows that rectifiers and converters are transforming electrical into thermal energy, which is afterwards emited into the environment. However, these devices are by far not the only equipment with this behavior. Prime movers, sensor and weapon systems as well as nearly every high power electrical system are dissipating heat into the ambience. This leads to an undesired temperature increase on board, which has the potential to affect the functionality and survivability of the ship. To avoid this dangerous behavior an active cooling of these components is necessary. A very efficient way to control the equipment temperature is to establish an active water cooling system.

Figure 4.5 shows the two closed systems A and B. Both systems are seperated from each other by a diathermic[3] wall and both are seperated from the environment by a perfect thermal insulation[4]. At time t_1 system A has the temperature T_A and system B has the temperature T_B. Temperature T_A is higher than T_B. Immediately after contact, it can be observed that the temperature in system A is falling and the temperature in system B is rising. At time t_2 both systems have reached the final temperature T, whereby $T_A > T > T_B$ [21].

[3] A diathermic wall allows heat, but not mass transfer [21].

[4] In reality a perfect thermal insulation is not possible, but it can be reached approximately [21].

This physical phenomena is called the *zeroth law of thermodynamics*. It basicaly says that two systems are in a thermal equilibrium if they do not transfer heat between each other although they would be able to do so. If two thermal connected systems have different temperatures, heat is transfered from the warmer to the colder system, until they have reached thermal equilibrium. This is the reason why heat transfer takes place [21].

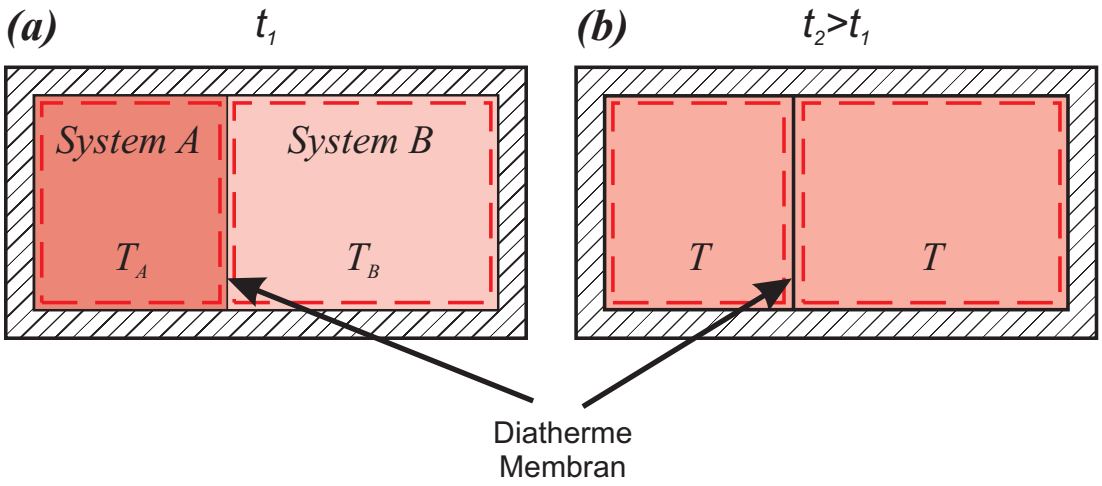

Figure 4.5: Thermal equilibrium: ***(a)*** Situation immediately after contact, ***(b)*** final situation after time t_2 [21, modified].

These circumstances lead to the conclusion that in order to decrease the temperature of a warm system, it is necessary to bring it into thermal contact with a colder system. This seemingly trivial knowledge is the base for cooling strategies in countless industrial applications, cars and electric power plants.
Also the cooling system of an AES works according to this principle. With reference to the example in figure 4.5, system A on board the vessel would be some kind of heat emitting equipment, for example a rectifier. System B would be the medium used to dissipate this heat from the equipment. In case of the AES the cooling medium is water. Figure 4.6 shows an example of a basic water cooling system.

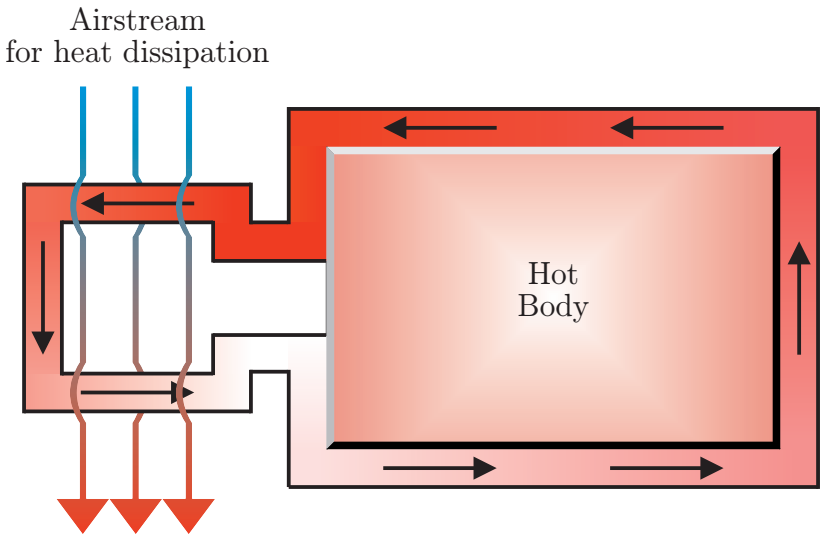

Figure 4.6: Example of an basic water cooling system.

Advantages of water as a cooling medium are especially the low price and the non-toxicity. Compared to air, water has a higher density, specific heat capacity, and thermal conductivity. This is the reason why water can transmit heat over greater distances with less volumetric flow and a lower temperature difference than air. A disadvantage of water is that it conducts electricity. That means that it can not get into direct contact with energized systems. It also accelerates corrosion of metal and is a medium for biological growth. However, most of these disadvantages can be avoided by the use of deionized water. Deionized water is normal tap water without the naturally dissolved minerals. It has a very low electrical conductivity and is a bad medium for biological growth. In combination with a corrosion preventive, deionized water can also be used in metalic environments.

An important difference between an AES cooling system and the example in figure 4.5 is that the cooling system of a vessel is not a closed system. That means that additional energy can be introduced into the system. This energy has to be removed by the cooling medium. In order to keep the system temperature within the desired range, it is necessary to release the stored energy from the water into the environment. Theoretical it would be possible to use seawater as cooling medium for the whole ship. The advantage of this solution would be that it would not be necessary to cool the hot water, because an inexhaustible reservoir of fresh cooling water would be available all the time. The problem with seawater as cooling medium is that it would accelerate corrosion dramatically. This would lead to shorter maintenance intervals and increased service demands. Therefore the

usage of seawater on board the vessel should be reduced to a absolute minimum. In order to take advantage of the cooling capacity of the seawater without dealing with the negative consequences, the AES employs two seperated cooling cycles. The primary cycle is an open one and uses seawater as cooling medium, whereas the secondary cycle is a closed loop and works with deionized water. Figure 4.7 shows a basic diagram of the cycles. In the secondary cycle the water is pumped through the whole system, where it transfers the energy away from the heat emitting equipment. Because it is a closed cycle, no mass transfer with the environment occurs in this loop. The primary cycle is used to dissipate the thermal energy from the secondary cycle. For this energy transposition a heat exchanger is employed. Since the primary cycle is an open loop, new cooling water can be introduced from the sea into the system. The warm water is dumped back into the ocean. The advantage of this methode is, that most of the systems on the ship do not get into direct contact with the seawater.

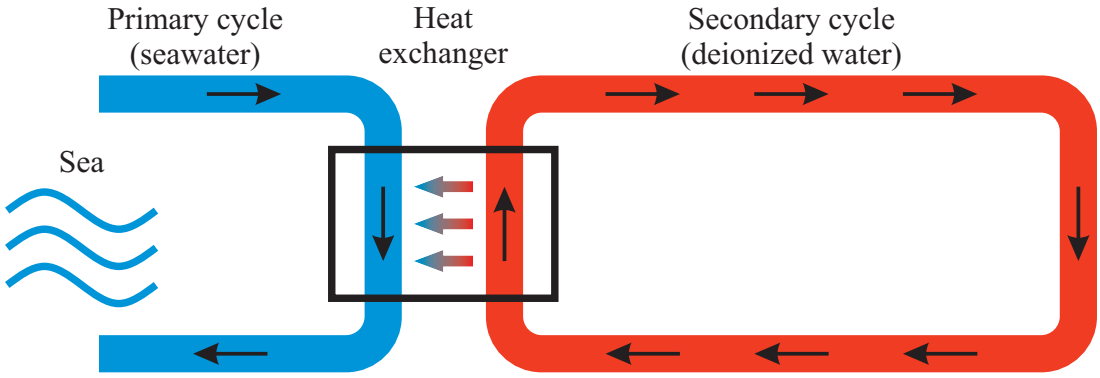

Figure 4.7: Basic diagram of the water colling cycles of an AES.

5 Modeling of the All-Electric Ship Cooling System

5.1 Configuration

As mentioned in the chapters above, an AES employes a vast number of devices that dissipate thermal energy during its regular operation. For this reason, rectifiers, PGMs and sensor and weapon systems require steady and reliable cooling. To fulfill this need on an AES, all devices which rely on additional cooling are parallel connected to the ship's cooling system. The maximum number of devices depends on the rating of the heat exchanger, which transfers the thermal energy from the secondary to the primary cooling cycle (figure 4.7) and the temperature of the cooling water. The heat exchanger rating is conditioned by its overall heat transfer coefficient, the heat transfer surface area and the mean temperature difference between the two fluids. Because of the parallel connection, the introduced cooling water has the same temperature for every device. The output cooling water temperature of the individual equipment depends on the dissipated energy and is therefore different for every device. Figure 5.1 shows the structure of the cooling system and how the equipment is connected to it. $T_1 - T_n$ are the temperatures in the individual devices. $T_{o1} - T_{on}$ refer to the output temperatures of the devices. T_x refers to the temperature conditions at the interfaces of the heat exchanger. *1* and *2* refer to the primary and secondary side whereas the subscripts i and o designate the fluid in- and outlet conditions. T_{amb} represents the ambient temperature in which the machines are employed. $\dot{m}_{x1}$ and $\dot{m}_{x2}$ are the mass flow rates in the primary and secondary cycle and $\dot{m}_1 - \dot{m}_n$ are the mass flow rates through the individual devices.

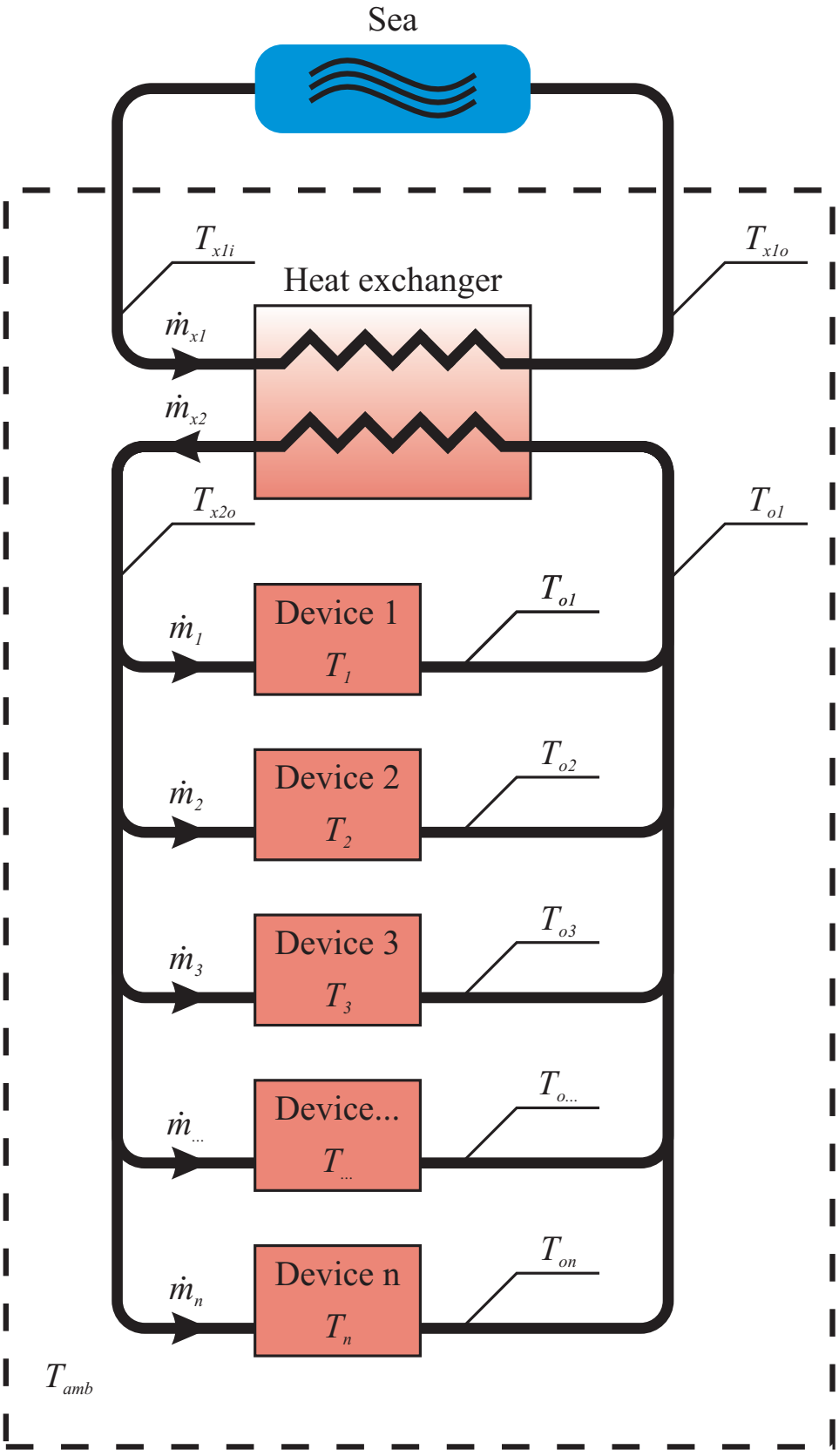

Figure 5.1: Modeling diagram of an AES cooling system.

5.2 System Equations

The goal of the simulation is to calculate the cooling water temperatures in

- the individual devices,
- at the outlets of the individual devices,
- and at the interfaces of the heat exchanger.

These points basically represent the whole cooling system. In order to simplify the modeling as much as possible, three simplifications were introduced:

1. The inlet water temperature of the primary heat exchanger cycle T_{x1i} is assumed to be not affected by the rest of the system.
2. The ambient temperature T_{amb} is assumed to be not affected by the rest of the system.
3. It is assumed that there is no energy drop in the pipes between heat exchanger and device and vice versa.

The first simplification is valid because of the virtual infinite amount of cooling water in the ocean. Even if the total available energy on board the vessel would be converted into heat (worst case scenario) and would be dissipated into the environment, it would have no measurable impact on the ocean's temperature. The second simplification was introduced because it can be assumed that the device has a good thermal insulation which keeps the energy dissipation through the equipment wall to small to affect the ambient temperature. The third simplification is valid because of the thermal insulation of the pipes which avoids a energy transfer through the pipe walls.
Considering these simplifications, it is possible to determine the total number of unknown temperatures for every system. This number is important because it defines the total number of system equations which are required to describe the system. With the information from above it can be said, that for every system the three heat exchanger temperatures T_{x1o}, T_{x2i} and T_{x2o} are unknown. This number is not affected by the number of devices in the cooling cycle. For every system with at least one energy dissipating device, these three temperatures are unknown. Additional to the three heat exchanger temperatures, every device in the cooling cycle increases the total number of unknown, by the temperature in

the device and the temperature at the outlet of the device. A cooling system with ten connected machines, for example, would therefore lead to 23 unknown temperatures. Ten device temperatures, ten device outlet temperatures and three heat exchanger temperatures. The only exception of this rule is a system with just one connected device. Because of simplification 3 from above, this would lead to a situation where the device outlet temperature T_{o1} would be equal to the inlet temperature of the secondary heat exchanger cycle T_{x2i}. In this special case just four temperatures would remain unknown.
This thesis will focus on a system with three devices. Although this is a very low number for a real AES cooling system, it is most suitable for modeling and simulation. A higher number of devices would increase the number of unknown temperatures and therefore the number of required system equations. This would lead to a higher calculation effort without adding any further value to the thesis. According to the statement above, a cooling system with three devices can be modeled with eleven different temperatures. Because of simplification 1 and 2, T_{x1i} and T_{amb} can be assumed to be not affected by the rest of the system. Therefore they can be set to a supposed and constant value. This leads to a total number of nine unknown temperatures, in a system with three devices. The unknown temperatures are the heat exchanger temperatures T_{x1o}, T_{x2i} and T_{x2o}, the device temperatures T_1, T_2, and T_3 and the outlet temperatures T_{o1}, T_{o2} and T_{o3}. In order to calculate these nine unknown temperatures, it is necessary to find nine system equations which describe the temperature behavior of the system. These equations can be found with knowledge about the laws of thermodynamics and with knowledge about the functionality of heat exchangers. The mathematical basics were introduced in chapter 4.
In order to find the system equations, it seems natural to start the search at the point where the energy is introduced into the system. Equation 4.1 shows, that the stored energy inside a system (figure 5.2) can only be changed by heat transfer through the boundaries and work done on or by the system. The energy inside an electrical system Q, is basically the difference between introduced electrical energy W_{in} and work done by the system W_{out}. Written as a rate, $\dot{Q}$ becomes:

$$\dot{Q} = \dot{W}_{in} - \dot{W}_{out} \tag{5.1}$$

For a rectifier, for example, Q would be the difference between AC input and DC output power. For a motor it would be the difference between the electric power that is driving the motor and the shaft work. On an AES this stored energy

can leave the system on two different ways. The first, and designated, way is the dissipation through the cooling system. The second one is the dissipation through the device wall.
The energy introduced into the cooling system can be calculated by unsing the simplified steady flow thermal energy equation 4.5.
The energy transfer through the device wall q_{wall} can be written as:

$$q_{wall} = hA(T_{amb} - T) \tag{5.2}$$

where h represents the heat transfer coefficient between the device and the ambient air. A is the device surface and T the device temperature. T_{amb} is the temperatures outside the device.

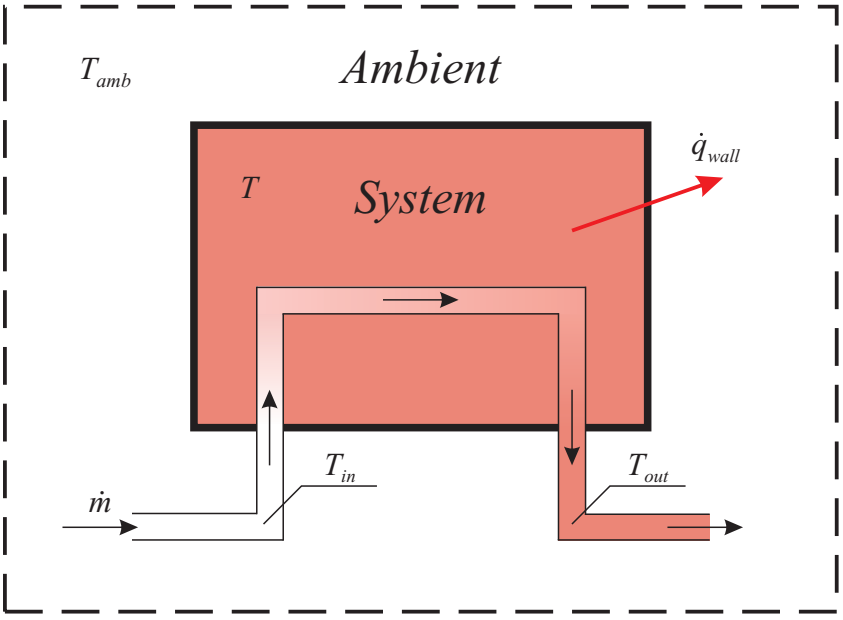

Figure 5.2: Energy change in a system.

With respect to the first law of thermodynamics and equations 5.1, 4.5 and 5.2, the energy change in device number one, of figure 5.1, can be written as:

$$\frac{dE_1}{dt} = M_1 c_{pfw} \dot{T}_1 = (\dot{W}_{in} - \dot{W}_{out}) + h_1 A_1 (T_{amb} - T_1) + \dot{m}_1 c_{pfw} (T_{x2o} - T_{1o}) \tag{5.3}$$

where:
M_1 represents the mass of the device in kg.

c_{pfw} represents the specific heat of deionized water at constant pressure in $^{\mathrm{J}}/_{(\mathrm{kg\,K})}$.
W_{in} represents the feeding power in W.
W_{out} represents the work done by the system in W.
h_1 represents the heat transfer coefficient between device one and ambient in $^{\mathrm{W}}/_{(\mathrm{m^2K})}$.
A_1 represents the surface of device one in m^2.

The same consideration is valid for device two:

$$\frac{dE_2}{dt} = M_2 c_{pfw} \dot{T}_2 = (\dot{W}_{in} - \dot{W}_{out}) + h_2 A_2 (T_{amb} - T_2) + \dot{m}_2 c_{pfw} (T_{x2o} - T_{2o}) \quad (5.4)$$

and device three:

$$\frac{dE_3}{dt} = M_3 c_{pfw} \dot{T}_3 = (\dot{W}_{in} - \dot{W}_{out}) + h_3 A_3 (T_{amb} - T_3) + \dot{m}_3 c_{pfw} (T_{x2o} - T_{3o}) \quad (5.5)$$

Further system equations can be found by taking a closer look at the energy transfer from the dissipating device, to the water of the cooling system. This transfer has significant similarities with the energy exchange inside a heat exchanger. Therefore it is valid to apply the heat exchanger equations from chapter 4.2.2 to this energy transfer.

$$\varepsilon_1 = \frac{T_{1o} - T_{x20}}{T_1 - T_{x2o}} \quad (5.6)$$

$$\varepsilon_2 = \frac{T_{2o} - T_{x20}}{T_2 - T_{x2o}} \quad (5.7)$$

$$\varepsilon_3 = \frac{T_{3o} - T_{x20}}{T_3 - T_{x2o}} \quad (5.8)$$

Because there is only one water stream the products of mass transfer and specific heats are cancelling each other.
The number of unknown temperatures in the system increases linear with the number of energy dissipating devices. For every additional energy source, two new unknown temperatures are introduced. For the modeling of the system this is not a problem, because above system equations are coupled to an individual

energy dissipating device. That means that for every further device in the system, two additional equations can be found by applying equations 5.3 to 5.5 and 5.6 to 5.8. System equations 5.9, 5.10 and 5.11 are not coupled to a energy source inside the system.
With equation 5.9 it is possible to calculate the inlet water temperature of the secondary loop of the heat exchanger T_{x2i}. It is basically a mixing equation for all the outlet streams of the individual devices:

$$T_{x2i} = \frac{\dot{m}_1 T_{1o} + \dot{m}_2 T_{2o} + \dot{m}_3 T_{3o}}{\dot{m}_1 + \dot{m}_2 + \dot{m}_3} \tag{5.9}$$

With every further energy source in the system, the equation expands by another term.
Another system equation can be found by applying equation 4.13, to the heat exchanger:

$$\varepsilon_x = \frac{\dot{m}_{x1} c_{psw} (T_{x1o} - T_{x1i})}{min\left\{(\dot{m}_{x1} c_{psw}), (\dot{m_{}}_{x2} c_{pfw})\right\} (T_{x2i} - T_{x1i})} \tag{5.10}$$

where:
ε_x represents the effectiveness of the heat exchanger.
c_{psw} represents the specific heat of seawater at constant pressure in $^{\mathrm{J}}/_{(\mathrm{kg\,K})}$.

The last missing system equation is the connection between the primary and secondary loop of the cooling system. Assumed that there is negligible energy transfer from the heat exchanger to the surroundings, a temperature difference between T_{x1i} and T_{x1o} has to have an impact on the secondary side of the cooling system and vice versa. This connection was already treated in chapter 4.2.1 and equations 4.8 and 4.9:

$$\dot{m}_{x1} c_{psw} (T_{x1o} - T_{x1i}) = \dot{m}_{x2} c_{pfw} (T_{x2i} - T_{x2o}) \tag{5.11}$$

This overall energy balance between the hot and cold fluids, can be applied for every heat exchanger regardless of size and type.
With equations 5.3 to 5.11 the system is entirely determined. By reorganizing these nine equations, all nine unknown temperatures can be computed.

5.3 State Space Representation

With the nine equations from chapter 5.2, the behavior of the system is determined and can be simulated. It turned out that an AES cooling system with three energy sources, is a linear time-invariant (LTI) third- order system. Such systems can be written as first order *state-variable models*, or just *state models*. For the analysis and design via state models, matrix mathematics is necessary. The most general state-space representation for a LTI-system with r inputs, p outputs and n state variables is written in the following form:

$$\begin{aligned} \dot{\mathbf{x}}(t) &= \mathbf{A}\mathbf{x}(t) + \mathbf{B}\mathbf{u}(t) \\ \mathbf{y}(t) &= \mathbf{C}\mathbf{x}(t) + \mathbf{D}\mathbf{u}(t) \end{aligned} \tag{5.12}$$

where boldface denotes vectors and matrices. In these equations,

$\mathbf{x}(t) = (n \times 1)$ state vector for an nth-order system;
$\mathbf{u}(t) = (r \times 1)$ input vector composed of the system input signals;
$\mathbf{y}(t) = (p \times 1)$ output vector composed of the defined output signals;
$\mathbf{A} = (n \times n)$ system matrix;
$\mathbf{B} = (n \times r)$ input matrix;
$\mathbf{C} = (p \times n)$ output matrix;
$\mathbf{D} = (p \times r)$ matrix that represents the direct coupling between the system inputs and the system outputs [22];

These two matrix equations of 5.12 are commonly referred to as *state equations* of a system. The first equation, which is a first-order matrix differential equation, is called *state equation,* and the state vector $\mathbf{x}(t)$ is its solution. The second one, a linear algebraic matrix equation, is called *output equation.* In the state equations of 5.12, only the first derivatives of the state variables may appear on the left side of the equation. No derivatives of the state or the input variables appear on the right side or in the entire output equation of 5.12. First-order coupled equations that model an LTI system and follow these rules are written in *standard form.* Of course, such systems may be written also in different forms but the standard form is the most common for technical applications [22].
In order to write equations 5.3 to 5.11 in standard form, it is necessary to rearrange them in a way, that the only unknown variables are T_1, T_2 and T_3. To avoid mistakes and to minimize the time effort for this rearrangement, it makes sense to use a computer for the calculations. Because of its powerful numeric and symbolic tools for discrete and continuous calculations, the computational

software Mathematica was used for the computations during this work. The corresponding code can be found in B. After the rearrangement equations 5.3, 5.4 and 5.5 can be written as:

$$\begin{aligned}
\dot{T}_1 &= \frac{1}{M_1 c_{pfw}}(\dot{Q}_1 + h_1 A_1(T_{amb} - T_1) + \dot{m}_1 c_{pfw}(T_{x2o} - T_{1o})) \\
\dot{T}_2 &= \frac{1}{M_2 c_{pfw}}(\dot{Q}_2 + h_2 A_2(T_{amb} - T_2) + \dot{m}_2 c_{pfw}(T_{x2o} - T_{2o})) \\
\dot{T}_3 &= \frac{1}{M_3 c_{pfw}}(\dot{Q}_3 + h_3 A_3(T_{amb} - T_3) + \dot{m}_3 c_{pfw}(T_{x2o} - T_{3o}))
\end{aligned} \tag{5.13}$$

And equations 5.6 to 5.11 can be written as:

$$\begin{aligned}
T_{1o} &= \varepsilon_1 * T_1 + (1 - \varepsilon_1) * T_{x2o} \\
T_{2o} &= \varepsilon_2 * T_2 + (1 - \varepsilon_2) * T_{x2o} \\
T_{3o} &= \varepsilon_3 * T_3 + (1 - \varepsilon_3) * T_{x2o} \\
T_{x1o} &= \frac{\varepsilon_x m_{x2} c_{pfw}(T_{x2i} - T_{x1i})}{m_{x1} c_{psw}} + T_{x1i} \\
T_{x2i} &= \frac{m_1 T_{1o} + m_2 T_{2o} + m_3 T_{3o}}{m_1 + m_2 + m_3} \\
T_{x2o} &= T_{x2i} - \frac{m_{x1} c_{psw}}{m_{x2} c_{pfw}}(T_{x1o} - T_{x1i})
\end{aligned} \tag{5.14}$$

The rearrangement shows that:

$$\begin{gathered}
T_{1o}(\varepsilon_1, \varepsilon_2, \varepsilon_3, \varepsilon_x, m_1, m_2, m_3, T_{x1i}, T_1, T_2, T_3) \\
T_{2o}(\varepsilon_1, \varepsilon_2, \varepsilon_3, \varepsilon_x, m_1, m_2, m_3, T_{x1i}, T_1, T_2, T_3) \\
T_{3o}(\varepsilon_1, \varepsilon_2, \varepsilon_3, \varepsilon_x, m_1, m_2, m_3, T_{x1i}, T_1, T_2, T_3) \\
T_{x1o}(\varepsilon_1, \varepsilon_2, \varepsilon_3, \varepsilon_x, m_1, m_2, m_3, m_{x1}, m_{x2}, c_{psw}, c_{pfw} T_{x1i}, T_1, T_2, T_3) \\
T_{x2i}(\varepsilon_1, \varepsilon_2, \varepsilon_3, \varepsilon_x, m_1, m_2, m_3, T_{x1i}, T_1, T_2, T_3) \\
T_{x2o}(\varepsilon_1, \varepsilon_2, \varepsilon_3, \varepsilon_x, m_1, m_2, m_3, T_{x1i}, T_1, T_2, T_3) \\
\dot{T}_1(\varepsilon_1, \varepsilon_2, \varepsilon_3, \varepsilon_x, m_1, m_2, m_3, c_{pfw}, A_1, h_1, c_1, M_1, Q_1, T_{x1i}, T_{amb}, T_1, T_2, T_3) \\
\dot{T}_2(\varepsilon_1, \varepsilon_2, \varepsilon_3, \varepsilon_x, m_1, m_2, m_3, c_{pfw}, A_2, h_2, c_2, M_2, Q_2, T_{x1i}, T_{amb}, T_1, T_2, T_3) \\
\dot{T}_3(\varepsilon_1, \varepsilon_2, \varepsilon_3, \varepsilon_x, m_1, m_2, m_3, c_{pfw}, A_3, h_3, c_3, M_3, Q_3, T_{x1i}, T_{amb}, T_1, T_2, T_3)
\end{gathered}$$

The next step is to define the state, input and output variables for the equations in 5.13. The three state variables, or more simply, *states,* are easy to determine because their derivatives are already part of the equations:

$$\begin{aligned} x_1(t) &= T_1 \\ x_2(t) &= T_2 \\ x_3(t) &= T_3 \end{aligned} \qquad \mathbf{x}(t) = \begin{bmatrix} T_1 \\ T_2 \\ T_3 \end{bmatrix} \tag{5.15}$$

The system input is the energy introduced into the system by the three devices:

$$\begin{aligned} u_1(t) &= \dot{Q}_1 \\ u_2(t) &= \dot{Q}_2 \\ u_3(t) &= \dot{Q}_3 \end{aligned} \qquad \mathbf{u}(t) = \begin{bmatrix} \dot{Q}_1 \\ \dot{Q}_2 \\ \dot{Q}_3 \end{bmatrix} \tag{5.16}$$

The system output vector consists of the remaining temperatures:

$$\begin{aligned} y_1(t) &= T_{1o} \\ y_2(t) &= T_{2o} \\ y_3(t) &= T_{3o} \\ y_4(t) &= T_{x1o} \\ y_5(t) &= T_{x2i} \\ y_6(t) &= T_{x2o} \end{aligned} \qquad \mathbf{y}(t) = \begin{bmatrix} T_{1o} \\ T_{2o} \\ T_{3o} \\ T_{x1o} \\ T_{x2i} \\ T_{x2o} \end{bmatrix} \tag{5.17}$$

Now that the state (5.15), input (5.16) and output (5.17) vectors are determined, it is necessary to find the related coefficients for these vectors. This separation can also be done by using Mathematica. For the state equation it is necessary to find for every entry in the state and input vector the related coefficient in equations 5.13. This leads to the system matrix **A** and the input matrix **B**:

$$\mathbf{A} = \begin{bmatrix} \dot{T}_1 coeff T_1 & \dot{T}_1 coeff T_2 & \dot{T}_1 coeff T_3 \\ \dot{T}_2 coeff T_1 & \dot{T}_2 coeff T_2 & \dot{T}_2 coeff T_3 \\ \dot{T}_3 coeff T_1 & \dot{T}_3 coeff T_2 & \dot{T}_3 coeff T_3 \end{bmatrix} \tag{5.18}$$

$$\mathbf{B} = \begin{bmatrix} \dot{T}_1 coeff \dot{Q}1 & \dot{T}_1 coeff \dot{Q}_2 & \dot{T}_1 coeff \dot{Q}_3 \\ \dot{T}_2 coeff \dot{Q}_1 & \dot{T}_2 coeff \dot{Q}_2 & \dot{T}_2 coeff \dot{Q}_3 \\ \dot{T}_3 coeff \dot{Q}_1 & \dot{T}_3 coeff \dot{Q}_2 & \dot{T}_3 coeff \dot{Q}_3 \end{bmatrix} \tag{5.19}$$

The entry in the first row and the first column in matrix **A**, stands for the related coefficient to T_1, in the system equation of $\dot{T}_1$, from the equations in 5.13. For the output equation in 5.12 it is necessary to determine the **C** and **D** matrix.

Similar to the procedure for the **A** and **B** matrix, the **C** and **D** matrix can be found by looking for the related coefficients to the state and input variables in the equations of 5.14:

$$\mathbf{C} = \begin{bmatrix} T_{1o}coeffT_1 & T_{1o}coeffT_2 & T_{1o}coeffT_3 \\ T_{2o}coeffT_1 & T_{2o}coeffT_2 & T_{2o}coeffT_3 \\ T_{3o}coeffT_1 & T_{3o}coeffT_2 & T_{3o}coeffT_3 \\ T_{x1o}coeffT_1 & T_{x1o}coeffT_2 & T_{x1o}coeffT_3 \\ T_{x2i}coeffT_1 & T_{x2i}coeffT_2 & T_{x2i}coeffT_3 \\ T_{x2o}coeffT_1 & T_{x2o}coeffT_2 & T_{x2o}coeffT_3 \end{bmatrix} \tag{5.20}$$

$$\mathbf{D} = \begin{bmatrix} T_{1o}coeff\dot{Q}1 & T_{1o}coeff\dot{Q}_2 & T_{1o}coeff\dot{Q}_3 \\ T_{2o}coeff\dot{Q}1 & T_{2o}coeff\dot{Q}_2 & T_{2o}coeff\dot{Q}_3 \\ T_{3o}coeff\dot{Q}1 & T_{3o}coeff\dot{Q}_2 & T_{3o}coeff\dot{Q}_3 \\ T_{x1o}coeff\dot{Q}1 & T_{x1o}coeff\dot{Q}_2 & T_{x1o}coeff\dot{Q}_3 \\ T_{x2i}coeff\dot{Q}1 & T_{x2i}coeff\dot{Q}_2 & T_{x2i}coeff\dot{Q}_3 \\ T_{x2o}coeff\dot{Q}1 & T_{x2o}coeff\dot{Q}_2 & T_{x2o}coeff\dot{Q}_3 \end{bmatrix} \tag{5.21}$$

Because there is no direct coupling between the system inputs and the system outputs, matrix **D** turned out to be a zero matrix.
The terms which are neither coefficients of the state nor coefficients of the input vector have to be added to the state and output equation.

$$\mathbf{OffsetAB} = \begin{bmatrix} Off\dot{T}_1 \\ Off\dot{T}_2 \\ Off\dot{T}_3 \end{bmatrix} \tag{5.22}$$

$$\mathbf{OffsetCD} = \begin{bmatrix} OffT_{1o} \\ OffT_{2o} \\ OffT_{3o} \\ OffT_{x1o} \\ OffT_{x2i} \\ OffT_{x2o} \end{bmatrix} \tag{5.23}$$

With the vectors and matrices from 5.15 to 5.23 the state equations can be written in standard form:

$$\begin{bmatrix} T_1 \\ T_2 \\ T_3 \end{bmatrix} = \begin{bmatrix} \dot{T}_1 coef f T_1 & \dot{T}_1 coef f T_2 & \dot{T}_1 coef f T_3 \\ \dot{T}_2 coef f T_1 & \dot{T}_2 coef f T_2 & \dot{T}_2 coef f T_3 \\ \dot{T}_3 coef f T_1 & \dot{T}_3 coef f T_2 & \dot{T}_3 coef f T_3 \end{bmatrix} \begin{bmatrix} T_1 \\ T_2 \\ T_3 \end{bmatrix} + \begin{bmatrix} \dot{T}_1 coef f \dot{Q}1 & \dot{T}_1 coef f \dot{Q}_2 & \dot{T}_1 coef f \dot{Q}_3 \\ \dot{T}_2 coef f \dot{Q}_1 & \dot{T}_2 coef f \dot{Q}_2 & \dot{T}_2 coef f \dot{Q}_3 \\ \dot{T}_3 coef f \dot{Q}_1 & \dot{T}_3 coef f \dot{Q}_2 & \dot{T}_3 coef f \dot{Q}_3 \end{bmatrix} \begin{bmatrix} \dot{Q}_1 \\ \dot{Q}_2 \\ \dot{Q}_3 \end{bmatrix} + \begin{bmatrix} Of f\dot{T}_1 \\ Of f\dot{T}_2 \\ Of f\dot{T}_3 \end{bmatrix}$$

$$\begin{bmatrix} T_{1o} \\ T_{2o} \\ T_{3o} \\ T_{x1o} \\ T_{x2i} \\ T_{x2o} \end{bmatrix} = \begin{bmatrix} T_{1o}coef f T_1 & T_{1o}coef f T_2 & T_{1o}coef f T_3 \\ T_{2o}coef f T_1 & T_{2o}coef f T_2 & T_{2o}coef f T_3 \\ T_{3o}coef f T_1 & T_{3o}coef f T_2 & T_{3o}coef f T_3 \\ T_{x1o}coef f T_1 & T_{x1o}coef f T_2 & T_{x1o}coef f T_3 \\ T_{x2i}coef f T_1 & T_{x2i}coef f T_2 & T_{x2i}coef f T_3 \\ T_{x2o}coef f T_1 & T_{x2o}coef f T_2 & T_{x2o}coef f T_3 \end{bmatrix} \begin{bmatrix} T_1 \\ T_2 \\ T_3 \end{bmatrix} + \begin{bmatrix} T_{1o}coef f \dot{Q}1 & T_{1o}coef f \dot{Q}_2 & T_{1o}coef f \dot{Q}_3 \\ T_{2o}coef f \dot{Q}1 & T_{2o}coef f \dot{Q}_2 & T_{2o}coef f \dot{Q}_3 \\ T_{3o}coef f \dot{Q}1 & T_{3o}coef f \dot{Q}_2 & T_{3o}coef f \dot{Q}_3 \\ T_{x1o}coef f \dot{Q}1 & T_{x1o}coef f \dot{Q}_2 & T_{x1o}coef f \dot{Q}_3 \\ T_{x2i}coef f \dot{Q}1 & T_{x2i}coef f \dot{Q}_2 & T_{x2i}coef f \dot{Q}_3 \\ T_{x2o}coef f \dot{Q}1 & T_{x2o}coef f \dot{Q}_2 & T_{x2o}coef f \dot{Q}_3 \end{bmatrix} \begin{bmatrix} \dot{Q}_1 \\ \dot{Q}_2 \\ \dot{Q}_3 \end{bmatrix} + \begin{bmatrix} Of fT_{1o} \\ Of fT_{2o} \\ Of fT_{3o} \\ Of fT_{x1o} \\ Of fT_{x2i} \\ Of fT_{x2o} \end{bmatrix} \tag{5.24}$$

6 Simulation of the All-Electric Ship Cooling System

Chapter 5 shows the modeling of an AES cooling system with three energy dissipating devices. With this model it is now possible to create a simulation of the entire system. Thermal simulation is a crucial part in developing an all-electric ship in order to practically manage both generated and wasted heat for satisfying cooling and heat signature requirements. Simulation at the system-level is important because a system containing fully optimized individual components usually does not result in the most effective system.
In the course of this research two simulations were created. The first simulation is a pure software simulation and was realized with Matlab / Simulink. The second one is a HIL simulation and was established with RSCAD from RTDS Technologies.

6.1 Simulation with Matlab / Simulink

Matlab (*mat*rix *lab*oratory) is a numerical computing environment and fourth-generation programming language for technical computing. It is an easy to use environment where problems and solutions are expressed in mathematical notation. Typical fields of application are:

- Math and computation
- Data acquisition
- Modeling and simulation
- Data analysis, exploration and visualization
- Application development, including graphical user interface building

Matlab's basic data element is an array that does not require dimensioning. Therefore it is particularly suitable for technical computing problems that involve matrix representations. Matlab's range of functions can be extended by a variety of application specific solutions called toolboxes [23]. One of these toolboxes is Simulink. Simulink is a Matlab extension for the modeling, simulation and analysis of dynamic systems. Its primary interface is a graphical block diagramming tool. The tight integration with the rest of the Matlab environment

combined with its clear user interface makes it to a widely used tool in the fields of control theory and digital signal processing for multidomain simulation.
For the simulation of the AES's cooling system the employment of Matlab and Simulink is very suitable. Because of the clear and intuitive system modeling in Simulink and the strengths of Matlab in matrix operations the implementation of the model can be done simple and in a reasonable amount of time.

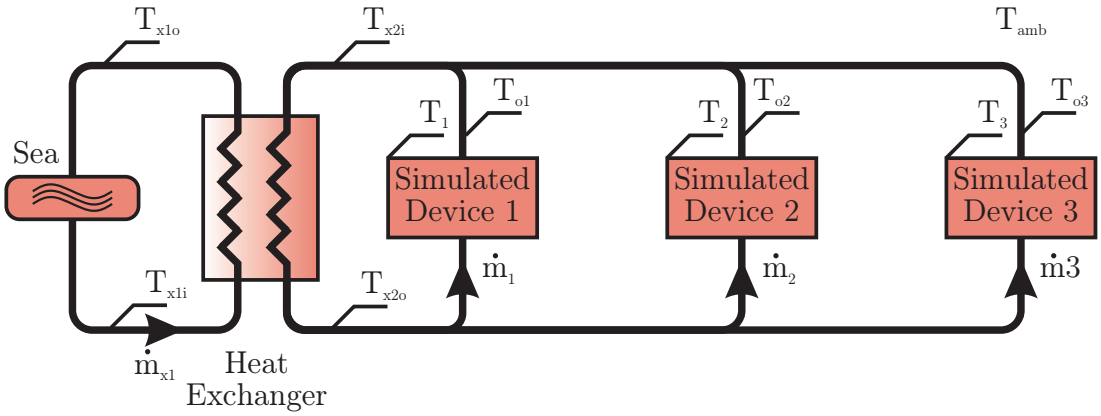

Figure 6.1: Configuration of the simulation environment.

For the simulation of the system shown in figure 6.1, it is necessary to define all parameters that can be found in the equations of 5.24. Some of the parameters like the mass flow rates, the device masses and the device surface areas were chosen random. The parameters are not related to real devices on an AES but they are suitable for the later HIL simulation. The heat transfer coefficient was set to $10\,\frac{\mathrm{W}}{\mathrm{m^2\,K}}$ which is a typical value for free convection between air and water. The specific heats c_1, c_2, c_3 were set to $435\,\frac{\mathrm{J}}{\mathrm{kg\,K}}$ which is a typical value for iron. c_{pfw} was set to $4183\,\frac{\mathrm{J}}{\mathrm{kg\,K}}$ and c_{psw} was set to $3993,7\,\frac{\mathrm{J}}{\mathrm{kg\,K}}$. A detailed table of these parameters and its values can be found in C.
The symbolical calculation of the A, B, C, D, $OffsetAB$ and $OffsetCD$ matrices was done in Mathematica. For the simulation it is necessary to transfer them as a variable into Matlab. This can be done by converting the Mathematica code to Matlab code. Fortunately Mathematica provides a function called *ToMatlab[]* that is suitable for this purpose. After this conversion the generated Matlab code can be transferred via copy/paste from Mathematica to Matlab.
The next step is the implementation of equations 5.24 into Simulink. The fact that Matlab is specialized in matrix operations makes the implementation rather simple. All the required mathematical operations are available in the Simulink

library. The matrices can be implemented as conventional constant blocks. The resulting block diagram is shown in figure 6.2. Of course the simulation would also be possible in a multitude of other programming languages, but the simplicity and clearness of the Simulink model brings certainly big advantages in matters of code readability and debugging.

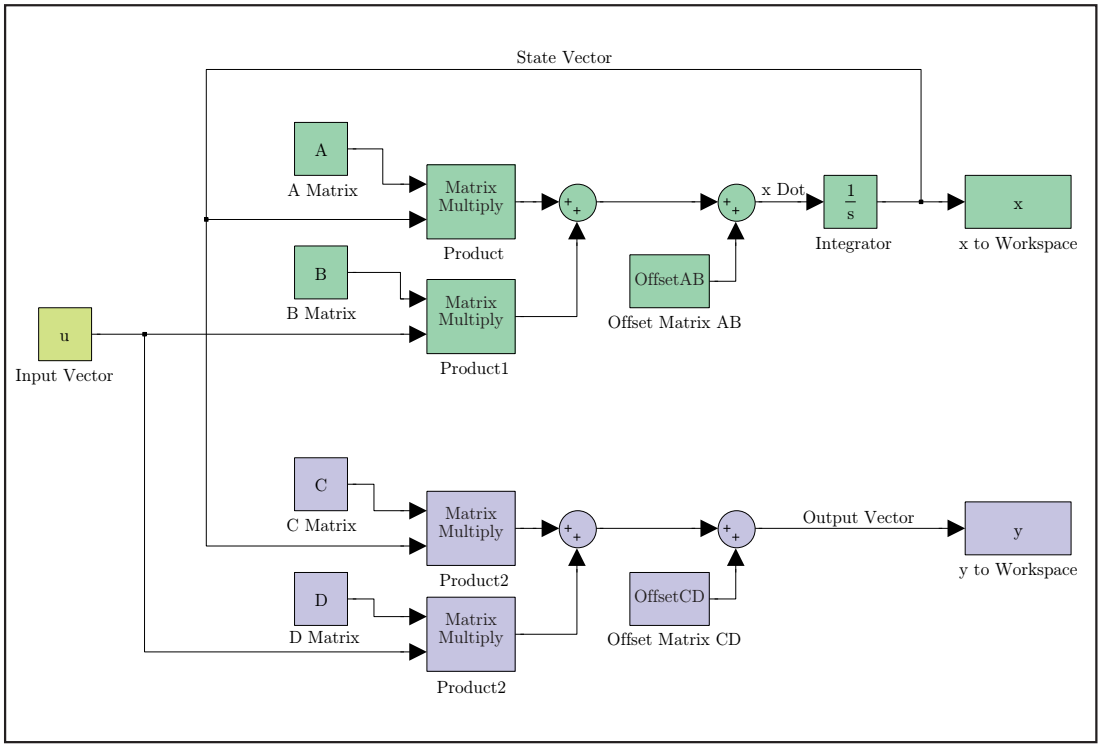

Figure 6.2: Simulink block diagram for equation 5.24.

In order to evaluate the simulation results it makes sense to think about the expected system behavior from figure 5.1:

1. Thermal energy is introduced into the cooling system at the devices. The temperature at the outlets increases.

2. The outlet water from all devices is mixed. The water temperature gets a value somewhere between the highest and the lowest device outlet temperature depending on the individual outlet temperatures and flowrates.

3. The warm water flows through the main heat exchanger where thermal energy is transfered to the primary cycle. The water temperature in the secondary cycle decreases, the temperature in the primary cycle increases.

With respect to this considerations it is now possible to evaluate the simulation results shown in figures 6.3 and 6.4.
At the beginning of the simulation all temperatures are equal at $T_{amb} = 20\,°\mathrm{C}$. To implement this behavior into the simulation it is necessary to set the initial condition of the integrator to this value. Immediately after activation all temperatures start to rise because of the introduced thermal energies $\dot{Q}_1$, $\dot{Q}_2$ and $\dot{Q}_3$. At the end of the simulation (simulation duration = 400 s) all temperatures are settled and have reached steady state.

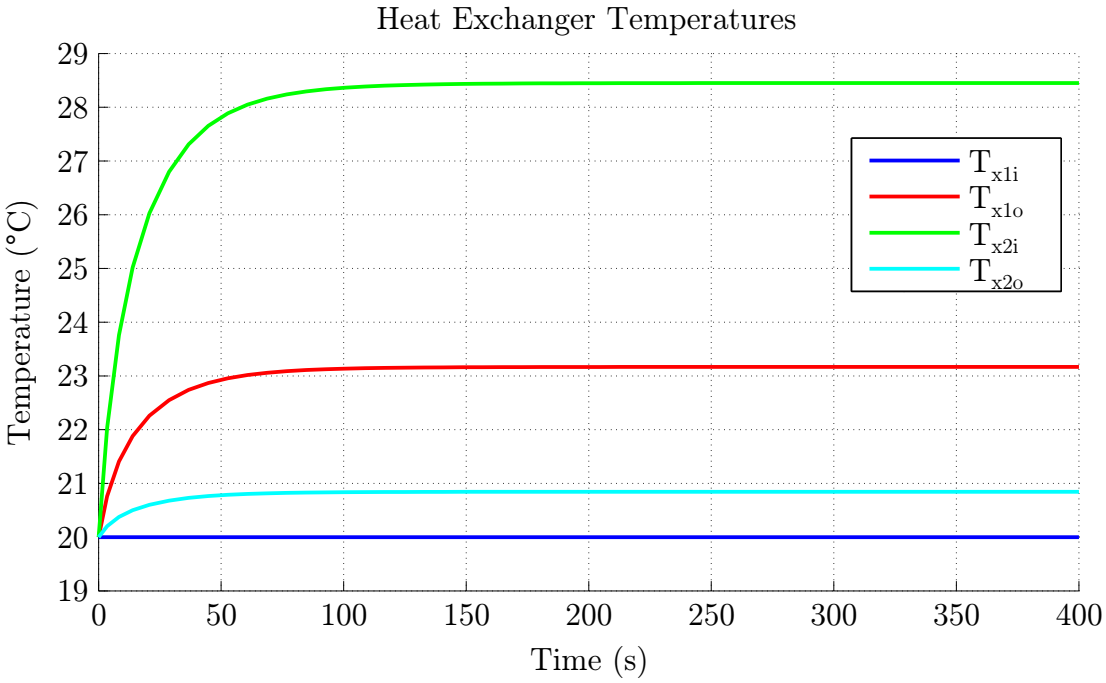

Figure 6.3: Simulation results: T_{x1i}, T_{xio}, T_{x2i}, T_{x2o}.

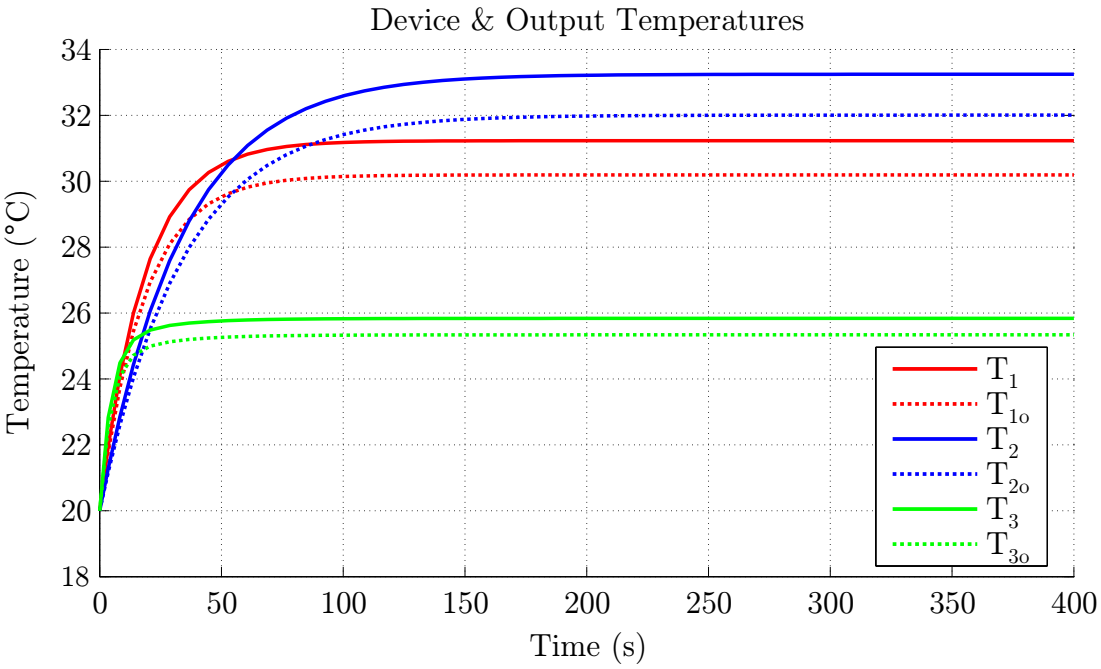

Figure 6.4: Simulation results: T_1, T_2, T_3, T_{1o}, T_{2o}, T_{3o}.

Figure 6.3 shows that the inlet temperature of the secondary cooling cycle is the highest of the four heat exchanger temperatures. This makes sense because this is the inlet where the hot drain water from the devices enters the heat exchagner. The lowest heat exchanger temperature is of course the inlet of the primary cycle. Because of simplification 1 of chapter 5.2 this temperature is constant at 20 °C. The major task of the heat exchanger is to transfer thermal energy from the secondary to the primary loop. Therefore the outlet temperature of the secondary cycle should be lower than the inlet temperature and the outlet temperature on the primary side should be higher than the inlet temperature. This behavior can be observed in the simulation result.
Figure 6.4 shows the device and the device outlet temperatures. It can be observed that the device outlet temperatures are closely connected to the particular device temperatures. The difference between these two temperatures is because of the heat exchanger effectiveness $\varepsilon < 1$. A perfect heat exchanger with $\varepsilon = 1$ would lead to $T_n = T_{no}$. The difference between the individual device temperatures depends on different factors like the introduced energy, the cooling water mass flow rate through the device or the device's mass.

6.2 Hardware in the Loop Simulation

Chapter 6.1 shows a conventional software simulation of an AES cooling system. For the underlying mathematical model of this simulation the energy dissipating devices were strong simplified and reduced to a couple of parameters. The problem with this simulation is that the devices coupled to a real AES cooling system are usualy very complex and therefore hard to model. This problem can be solved by applying an HIL simulation on the cooling system.
HIL simulation is a technique that is used in the development and test of complex real-time systems. It is a procedure in which an embedded system, like an electronic control unit or a real mechatronic device, is connected to a HIL-simulator which is emulating the system's real environment. The concept of hardware-simulation coupling has been existing for several years and is today a widely used concept in different fields of engineering. Two types of HIL simulation can be distinguished. The *plant simulation* where the mathematical model of the control object, called plant, is running on a general purpose computer which is connected to a real controller, and the *controller behavior simulation* where the prototype of a control program runs on a general purpose computer which is connected to a real device. The connection between hardware and simulation is usualy made via a data acquisition (DAQ) board. Reasons that lead to the development of HIL simulation systems are:

- Systems can be tested without compromissing hardware or jeopardizeing people's health. Safety- critical components can be tested without danger.
- HIL tests are cost-efficient. A test setup is easier and faster to configure in a virtual environment than in a real one. Fewer hardware components lead to cost savings.
- A high degree of automation is feasible.
- A virtual environmet can be easily modified, so a real control can be tested in different control loops. On the other hand, a real control loop can be easily tested with different simulated controllers or control algorithms. Ambient conditions can be simulated by simple parameter changes.
- A high degree of repeatability.
- If parts of a system are too complex to model they can be replaced by the real hardware.

- The embedded hardware can accelerate the simulation [24].

In the context of engineering complex systems such as a cooling system for an AES, HIL simulation is a suitable tool for system analysis, optimization, validation and verification. In a typical HIL simulation, system dynamics are emulated by mathematical models and executed by a real-time processor. A process I/O or DAQ unit allows the connection of sensors and actuators to a testbed.
For the HIL simulation of the AES cooling system a physical thyristor bridge rectifier was implemented into the simulation. This choice was made because of the high number of energy converters on board a vessel. Figure 6.5 shows the configuration of the testbed. The green devices are physical hardware components, the red devices are simulated. The initial situation for the HIL simulation is exactly the same than for the simulation in chapter 6.1. The only difference is that the third energy dissipating device is replaced by the real physical rectifier. This change implicates the necessity to monitor the in- and output water temperatures as well as the water flow through the device. Another characteristic of a HIL simulation is that the simulation result has an influence on the hardware. Depending on the outlet water temperatures of the real and simulated devices the inlet temperature of the rectifier has to be adapted to the calculated value. Therefore it is necessary to implement a thermal amplifier to the testbed which provides the inlet temperature for the rectifier. On this way the hardware influences the simulation and the simulation result has a direct impact on the behavior of the hardware.

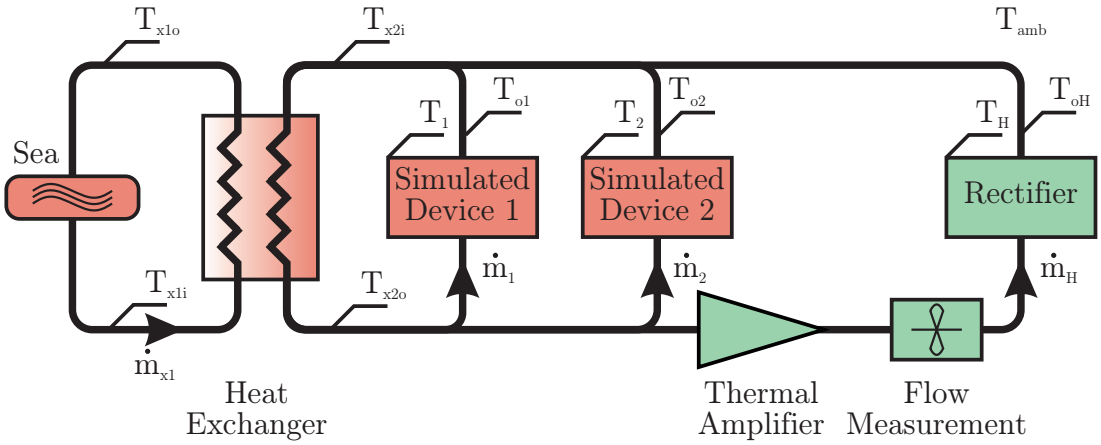

Figure 6.5: Configuration of the HIL testbed.

For the connection between hard- and software DAQ boards are necessary to feed the rectifier temperatures to the simulation and the resulting control signal

to the thermal amplifier. Because of the time-critical nature of HIL simulations it is essential to run the simulation in a real-time environment. This basic requirement was fulfilled by running the simulation on the RTDS located at the CAPS. The RTDS from RTDS Technologies is designed specifically to simulate electrical power systems and to test physical equipment such as control and protection devices. The main interface with this special hardware is RSCAD which allows the user to perform all of the necessary steps to prepare and run simulations, and to analyze the results [25, 26].

The implementation of the mathematical model from equations 5.24 into the RSCAD environment is basically identical to the implementation into Simulink. The only difference is that T_{x2o} and T_{Ho} are physical inputs from the hardware under test. As explained in chapter 6.1 the A, B, C, D, $OffsetAB$ and $OffsetCD$ matrices of equation 5.24 were computed in Mathematica and converted to Matlab code. For the HIL simulation with RSCAD this procedure is not practicable because Mathematica does not provide a function to convert Mathematica to RSCAD code. This problem can be solved by using Mathematica to calculate the numerical values of the matrices and generate a *.txt* file with the solutions. This .txt file can be imported into the RSCAD environment where it can be used for the following simulation.

Because of time limitations it was not possible to run the actual tests in the course of the project. Therefore the results of the tests are not part of this thesis and have to stay subject of further work.

Part III

Testbed for the Hardware-in-the-Loop Simulation

7 Configuration of the Testbed

An overview on the testbed configuration was already given in chapter 6.2. In this chapter the device under test, the measurement setup and the thermal amplifier are introduced in detail. The entire testbed described in this chapter was realized in the electromechanics laboratory of the CAPS in Tallahassee, Florida. The purpose of this validation effort is not solely to compare simulation and experimental results, but also to analyze and develop statistical parameters that provide a quantitative assessment of how good the model represents an actual system over a range of operating conditions. Such validation improves the usage of the system model so that the user can know better when to employ the model and what level of confidence to have in it. This is important on an AES where the simulation might be used to verify whether the cooling loop within the complete system has enough potential to prevent overheating of electronic devices during transients, or whether the system is capable of handling additional loads without having to modify the existing system configuration.

7.1 Rectifier

The hardware chosen for this HIL simulation is the mobile six pulse bridge rectifier shown in figure 7.1.

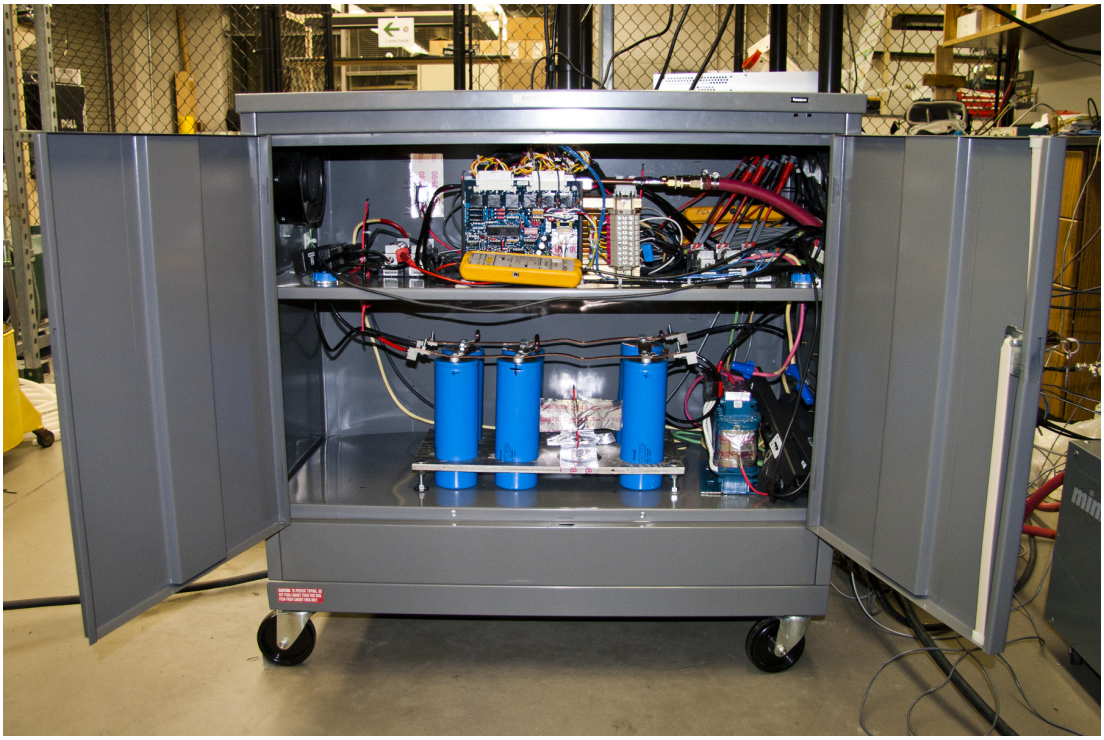

Figure 7.1: Frontal view of the thyristor bridge rectifier.

It is rated for a maximum output power of 50 A direct current. Figure 7.2 shows its main power path and table 1 the ratings of its main components. The device has two separated power inputs. One 3-phase AC input for the transformation power and one single phase 120 V / 60 Hz input for the control power. The bridge rectifier is built up of three *SEMIKRON SKKT92* thyristor modules. Each module consists of two thyristors connected in series. The firing angle of the semiconductors, and with it the output voltage, can be controlled over a $0 - 5$ V DC input, which can be enabled by an on-off switch.
In order to keep the cabinet below a critical operating temperature the thyristor modules have to be cooled. Originally the rectifier was designed to be air cooled. In order to use it for the HIL test setup it was necessary to add a water heat sink to the device. On this water heat sink all three thyristor modules were mounted. Figure 7.3 shows a top view on the upper partitionment of the rectifier with the thyristor bridge, the water heat sink, the in- and output fuses and the voltage and current probes.

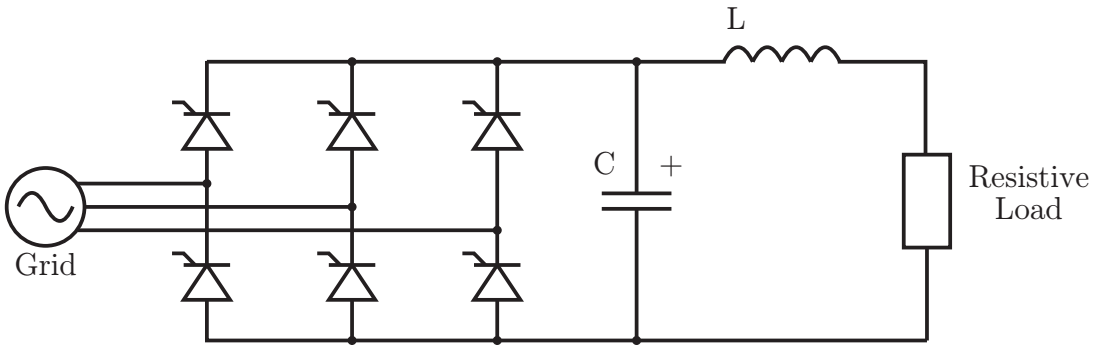

Figure 7.2: Six pulse bridge rectifier: Main power path.

Component	Rating
Input fuses	70 A
Thyristor bridge (per module)	150 A (maximum for continuous operation)
Capacitor (C)	15 mF
Inductor (L)	1, 2 mH
Output fuses	50 A
Resistive Load (R)	7, 2 Ω

Table 1: Six pulse bridge rectifier: Main power path components.

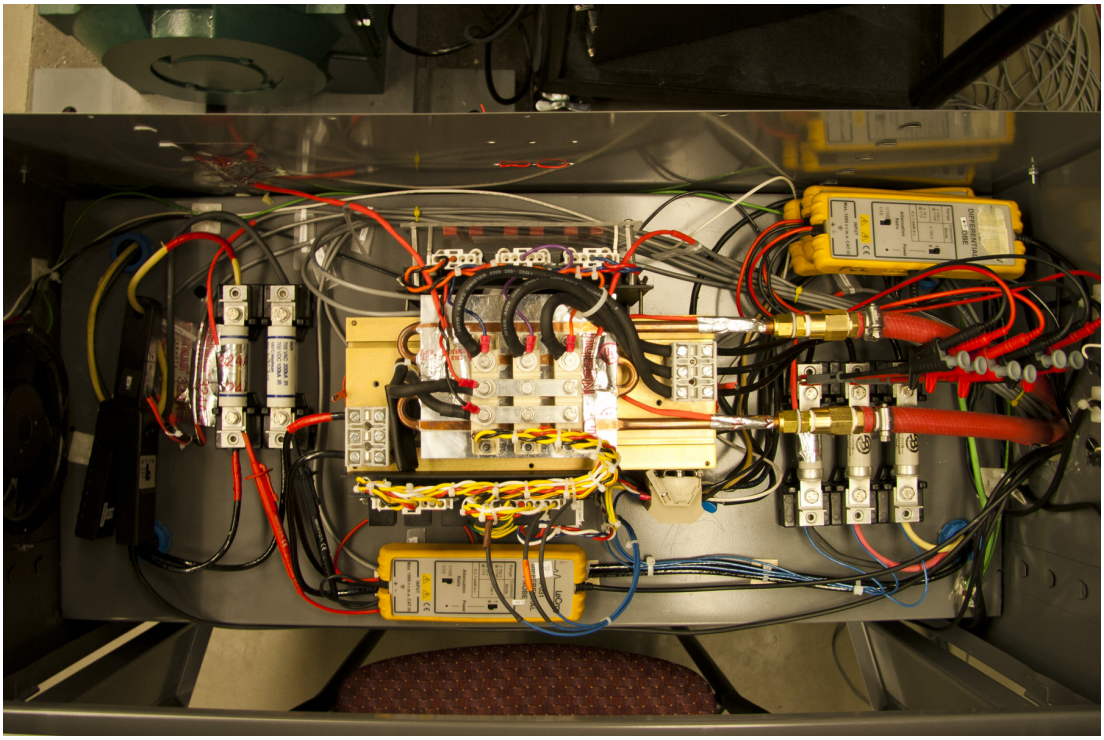

Figure 7.3: Top view of the thyristor bridge rectifier.

7.2 Measurement Setup

To establish a HIL simulation it is necessary to capture and evaluate a multitude of data. In the course of this simulation different temperatures, a mass flow rate, voltages and currents were captured.

7.2.1 Temperature

The temperature measurement is of particular importance for the execution of this HIL simulation. T_{x2o} and T_{Ho} have to be measured and fed back into the simulation. In addition, the rectifier was equipped with 15 temperature sensors all over the device to monitor the temperature behavior of the rectifier during operation. Though, these additional sensors are not necessary for the simulation they can be used for security purposes like an emergency shutdown.
For the temperature measurement negative temperature coefficient (NTC) resistors were used. Thermistors are semiconductor devices that exhibit a negative coefficient of resistance with temperature. A typical resistance/temperature ratio is 4 % resistance change per °C. They are available for different temperature regions and in different packages, ranging from tiny glass beads to armored probes. Thermistors intended for accurate temperature measurement typically have a resistance of a few thousand ohms at room temperature. They are a good choice for temperature measurement in the range of $-50\,°C$ to $300\,°C$ and are available with tight conformity ($0,1$-$0,2\,°C$) to standard curves. Further advantages are their large coefficient of resistance change and their low price. When compared with other methods of temperature measurement, thermistors provide simplicity and accuracy, but they suffer from selfheating effects, fragility, and a narrow temperature range. The self-heating effect is an error which can occur when the power applied to a thermistor exceeds its ability to dissipate that power to the environment. In such a case the not dissipated power leads to an increase of the temperature in the probe. A typical small thermistor probe might have a dissipation constant of $1\,mW/°C$. That means that for a maximum measurement error of $1\,°C$, the highest acceptable measurement power I^2R is $1\,mW$. Attention should be paid to the fact that R is a function of the temperature. That means that the measurement power will increase with higher temperatures. In order to that, thermistors should nearly be used under zero power conditions, if they are used for temperature measurements [27].
The thermistor temperature/resistance relation depends on the used semicon-

ducting material. It has clearly nonlinear characteristics. Commonly the exact behavior of the thermistor is determined by the manufacturer through tests and is given to the user in form of a lookup table [28]. Figure 7.4 shows the resistance behavior of the used thermistor-type, in the temperature range between -55 °C and 120 °C.

In order to get accurate results, it is necessary to detect and adjust the systematic fault of each single thermistor. A comfortable method for this task is to use the thermistor calibration tool of National Instruments (NI). For this calibration it is necessary to know the Steinhart-Hart parameters of the used thermistors, as well as the resistances at, at least, two different temperatures. For the thermal characterization of the thyristor bridge, the thermistors were calibrated with two water baths. One bath was filled with ice water, the other one with boiling water. On this way the reference temperatures of 0 °C and 100 °C were provided. The small failure, due to the fact that the test bed was not exactly on sea level but around 20 m above, was neglected.

In order to capture the temperature at the heat sink's in- and outlet, the probes were attached with a heat resistant tape on the points of interest. To make sure that the probes detect only the temperature of the heat sink and not the temperature of the surrounding environment, the tape was covered with a thermal insulation.

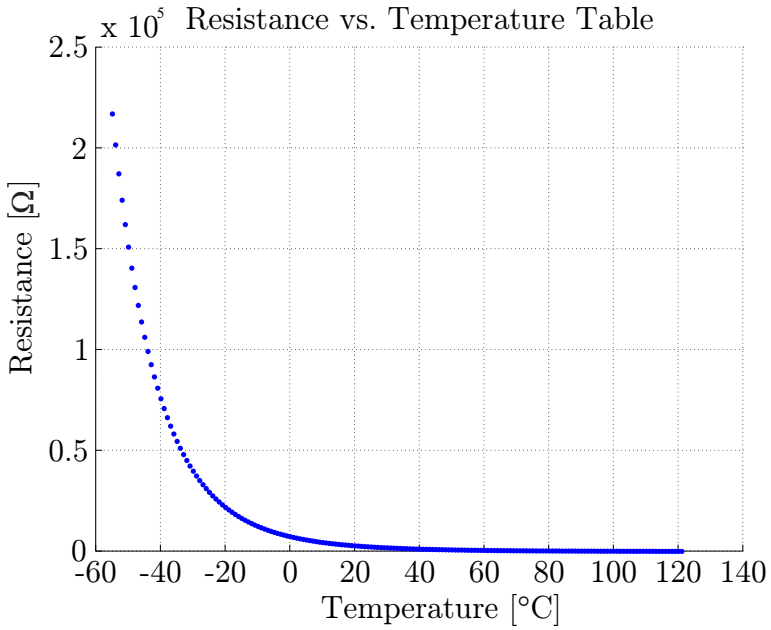

Figure 7.4: Resistance vs. temperature table: Thermistor typ 44004RC [1].

7.2.2 Water Flow

Like the temperature measurement, the water flow measurement is of great importance for the HIL simulation. For the simulation it is necessary to detect the water flow $\dot{m}_H$ through the device. This detection was realized with the low-flow meter *Omega FPR300*. The Omega FPR300 is a versatile impeller flowmeter with optical rotation detection. It was driven by a standard 12 V power supply. The 12 V pulse output was directly fed into the RTDS. Via a RSCAD program the pulses were counted and the water flow was calculated and fed into the simulation.

7.2.3 Voltage and Current

Other than the temperature and mass flow measurement, the voltage and current measurement is not required for the HIL simulation. Nevertheless, the measurement makes sense in order to control and monitor the behavior of the rectifier during operation. In the course of this project the following voltages and currents were measured:

- AC voltage between A and B (input),
- AC voltage between A and C (input),
- AC voltage between B and C (input),
- the currents over A, B and C (input),
- the DC voltage (output),
- the DC voltage (output).

For the voltage measurement *Lecroy AP031* probes were used. The currents were detected contactless with *Tektronix A622* probes. The results were fed directly into the RTDS.

7.2.4 Data Acquisition

Other than the flow measurement, which is fed directly into the RTDS, the temperature, voltage and current measurement is read out over a *NI-PXI-1010* chassis. This chassis combines a 8-slot PXI subsystem with a 4-slot SCXI subsystem

to offer a complete solution for signal conditioning applications. The PXI partition accepts an embedded controller and a wide variety of peripheral modules such as multifunction I/O, digital I/O, and instrument modules. The four SCXI slots integrate signal conditioning modules into the PXI system. These modules provide analog and digital input conditioning [29]. For the testbed measurement a *NI-SCXI-1102* module was employed. These modules are for signal conditioning of thermocouples, low-bandwidth volt and millivolt sources and 4 to 20 mA current sources. One NI-SCXI-1102 module has 32 differential analog input channels and one cold-junction sensor channel. Every channel has an amplifier with a selectable gain of 1 or 100. The inputs can be multiplexed to a single output, which drives a single DAQ device channel [30]. For the connection between the leads and the NI-SCXI-1102 module, a *NI-SCXI-1300* terminal block was used. In order to detect the rectifier temperature as accurate as possible, a four-wire wiring was chosen to connect the thermistors. In the four-wire configuration one pair of wires is used to deliver the excitation current to the thermistor and another pair is used to sense the voltage across the thermistor. Due to the high input impedance of the differential amplifier, negligible current flows through the sense wires. This results in a very small lead-resistance voltage drop error. A disadvantage of this configuration is the greater number of field wires required [2]. Figure 7.5 shows a wiring diagram for a temperature measurement in four-wire configuration. R_{L1}, R_{L2}, R_{L3} and R_{L4} represent the lead resistances and R_T represents the resistance of the thermistor. R_{L1}, R_{L2}, R_{L3} and R_{L4} are not required to be equal.

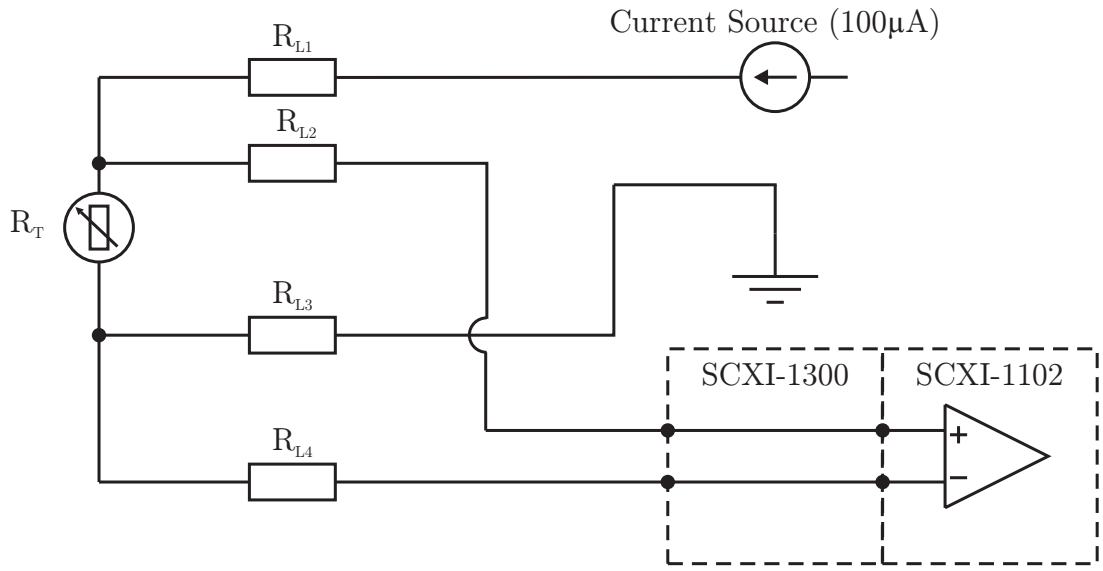

Figure 7.5: Resistive sensor connected in a four-wire configuration [2, modified].

The sampling rate for the temperatures was 20Hz whereas the sampling rate for every other measurand was 20kHz.
To provide the excitation current of 100 μA, a *Lake Shore 120CS* current source was used.

7.3 Thermal Amplifier

As mentioned above, a characteristic of a HIL-simulation is that the simulation result has an impact on the real world. In the AES cooling system HIL-simulation, this impact is the inlet temperature for the rectifier. To execute the HIL-simulation it is therefore necessary to manipulate this temperature. For this purpose a thermal amplifier was employed, which is able to provide a designated fluid temperature for a connected process.
The used hardware was a modified version of a *Mokon Minitherm.* The modification was required because for the HIL-simulation it was necessary to adjust the process temperature of the device with the RTDS. For that reason the standard controller was removed and was replaced by two solid state relays. These relays, which were controlled by the RTDS, were used to open the drain valve, when the process temperature was to high, and to turn on the heater, when the process temperature was to low.
A flow scematic of the thermal amplifier is shown in figure 7.6.

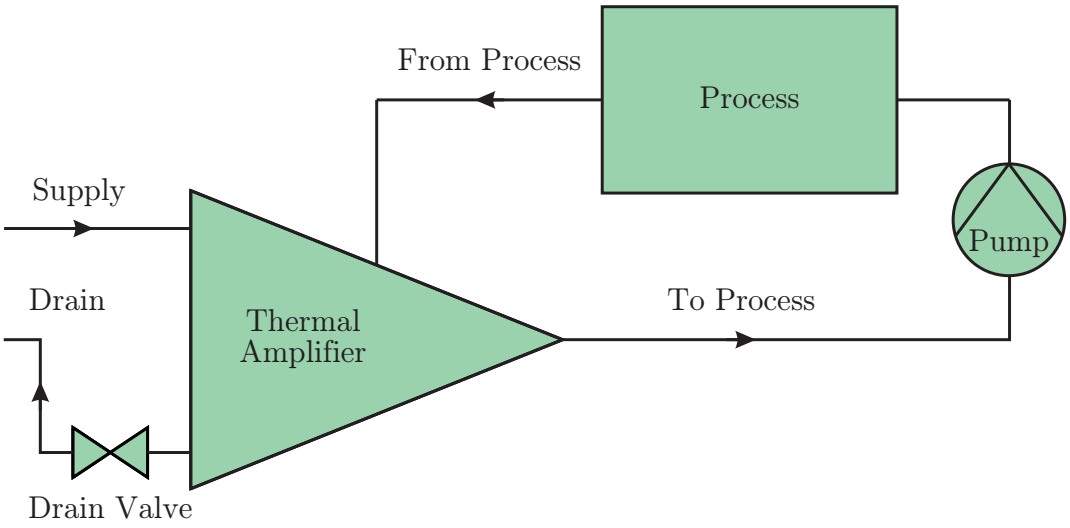

Figure 7.6: Flow schematic of the thermal amplifier.

Part IV

Results and Findings

8 Conclusions and Recommendations for Future Research

In the course of this thesis the theoretical basis for the modeling of an AES cooling system was introduced. Based on these theoretical principles, a model of such a cooling system with three energy dissipating devices was established. With the use of the first law of thermodynamics and the heat exchanger effectiveness, it was shown that such a system can be represented with a set of nine equations with nine unknown temperatures. With the use of Wolfram Mathematica, which is a suitable tool for symbolical calculations, these equations were reorganized and transfered into a state space representation. Although this transformation was not a necessity it was chosen to ease the implementation into the simulation software. The resulting model was implemented and validated in a Matlab / Simulink simulation, which turned out to be a suitable software environment for such kind of simulations. The result of this simulation was a concrete representation of the temperature behavior of the system.
In order to evaluate the conventional simulation results the generation of a HIL-

simulation was illustrated. This simulation was executed in the real-time environment RSCAD which is the software environment for the RTDS. Further the configuration of the HIL-testbed was shown.
As mentioned in chapter 6.2, it was due to time limitations not possible to run the actual HIL-simulation so far. This is of course the next step in the course of this research. The HIL-simulation should be realized and the results should be compared with the Matlab / Simulink simulation with the same set of parameters. On this way the mathematical model can be evaluated and the divergence between the simulation and the real behavior of the system can be determined.
A useful improvement for further projects would be the reduction of involved software. For this reason it should be tried to do the symbolical calculations with Matlab instead of Wolfram Mathematica. This reduction would lead to time and cost optimizations and could lead to more clarity in the modeling and simulation procedure.
The next step in the evolution of this topic could be a real-time thermal-electrical co-simulation. Basicaly a experiment where, additionaly to the thermal behavior of the system, also the electrical behavior of the device under test is part of the HIL-simulation. Such a system-level thermal-electrical co-simulation could provide useful insights on how the complete system would run in both electrical and thermal points of view under different operation modes. The comparison between theoretical and experimental data and its analysis promises a more useful system model for the AES.
The HIL-simulation described in this thesis was the first of its kind on the CAPS. Therefore the test was realized in a rather small scale. For better and more realistic results the experiment could be adapted and repeated in a bigger scale in the CAPS High Bay facility. This facility has a unique setup and can be used to test various high power motors and other high power concepts. Among other equipment the facility is equipped with two $2,5\,\mathrm{MW}$ General Electrics induction motors driven by four-quadrant pulse-width modulation variable speed drives from Toshiba. The heat dissipation of the whole system is realized by a series of heat exchangers which transfer the heat from the internal closed cooling loop to an external cooling tower. This impressive arrangement would be eminently suitable for a real-time system-level thermal-electrical co-simulation in a scale which would be comparable to the proportions of a real AES.

Bibliography

[1] Measurement Specialties, "Datasheet: 44004rc precision epoxy ntc thermistor," 2008.

[2] National Instruments Corporation, "Scxi-1581 user manual," 2006.

[3] George Washington, *The Writings of George Washington from the Original Manuscript Sources 1745-1799. vol.23*, Washington D.C., 1937.

[4] US Navy web staff. The u.s. navy. [Online]. Available: http://www.navy.mil/navydata/nav_legacy.asp?id=146 [Accessed: 05.11.2012]

[5] Office of naval research home page. [Online]. Available: http://www.onr.navy.mil/ [Accessed: 05.11.2012]

[6] Esrdc: Electric ship research and development consortium, thrusts. [Online]. Available: http://www.esrdc.com/thrusts.html [Accessed: 05.11.2012]

[7] Esrdc: Electric ship research and development consortium. [Online]. Available: http://www.esrdc.com/index.html [Accessed: 05.11.2012]

[8] Esrdc: Electric ship research and development consortium. [Online]. Available: http://www.esrdc.com/technical.success.html [Accessed: 06.11.2012]

[9] M. A. Pruske, "Thermal-electrical co-simulation of shipboard integrated power systems on an all-electric ship," Ph.D. dissertation, University of Texas at Austin, Austin and Texas, 2009.

[10] P. E. Paullus, "Creation of a modeling and simulation environment for thermal management of an all-electric ship," Ph.D. dissertation, University of Texas at Austin, 2007.

[11] C. R. Holsonback, "Dynamic thermal-mechanical-electrical modeling of the integrated power system of a notional all-electric naval surface ship," Ph.D. dissertation, University of Texas at Austin, 2007.

[12] Uss arleigh burke: Ship characteristics. [Online]. Available: http://www.public.navy.mil/surflant/ddg51/Pages/Characteristics.aspx [Accessed: 22.11.2012]

[13] M. S. Pierce, "Dynamic thermal modeling and simulation framework: Design of modeling techniques and external integration tools," Ph.D. dissertation, University of Texas at Austin, 2009.

[14] US Department of Defense, "Military critical technologies list: Section 7," 2005.

[15] H. Cortes, "Theoretical and experimental simulation of all electric ship propulsion system cooling with hot stream energy scavenging," Ph.D. dissertation, Florida State University, 2008.

[16] O. Faruque, V. Dinavahi, M. Sloderbeck, and M. Steurer, "Geographically distributed thermo-electric co-simulation of all-electric ship," 2009.

[17] (2007) Next generation integrated power system: Ngips technology development roadmap. [Online]. Available: http://www.dtic.mil/cgi-bin/GetTRDoc?AD=ADA519753 [Accessed: 03.12.2012]

[18] N. Mohan, T. M. Undeland, and W. P. Robbins, *Power electronics: Converters, applications, and design*, 3rd ed. Hoboken and NJ: Wiley, ca. 2007.

[19] F. P. Incropera and D. P. DeWitt, *Fundamentals of heat and mass transfer*, 6th ed. Hoboken and NJ: Wiley, 2007.

[20] H. Martin, *Heat exchangers*. Washington: Hemisphere Publ. Corp, 1992.

[21] W. Geller, *Thermodynamik für Maschinenbauer: Grundlagen für die Praxis*, 4th ed., ser. Springer-Lehrbuch. Berlin and Heidelberg: Springer-Verlag Berlin Heidelberg, 2006.

[22] C. L. Phillips, J. M. Parr, and E. A. Riskin, *Signals, systems, and transforms*, 3rd ed. Upper Saddle River and NJ: Pearson/Prentice Hall, 2008.

[23] R. C. Gonzalez, R. E. Woods, and S. L. Eddins, *Digital Image processing using MATLAB*. Upper Saddle River and N.J: Pearson Prentice Hall, 2004.

[24] C. Köhler, *Enhancing embedded systems simulation: A Chip-Hardware-in-the-loop simulation framework*, 1st ed. Wiesbaden: Vieweg + Teubner, 2011, 2011.

[25] Power system simulator hardware | rtds technologies. [Online]. Available: http://www.rtds.com/hardware/hardware.html [Accessed: 19.01.2013]

[26] Power system simulator software | rscad software suite | rtds technologies. [Online]. Available: http://www.rtds.com/software/rscad/rscad.html [Accessed: 19.01.2013]

[27] P. Horowitz and W. Hill, *The art of electronics*, 2nd ed. Cambridge: Cambridge University Press, 1998.

[28] E. Böhmer, D. Ehrhardt, and W. Oberschelp, *Elemente der angewandten Elektronik: Kompendium für Ausbildung und Beruf ; mit einem umfangreichen Bauteilekatalog*, 16th ed. Wiesbaden: Vieweg + Teubner, 2010.

[29] National Instruments Corporation, "Ni pxi-1010 chassis user manual: Combination chassis for pxi, compactpci, and scxi modules," 2004.

[30] ——, "Scxi-1102/b/c user manual," 2006.

A List of Abbreviations

AES	All Electric Ship
CAPS	Center for Advanced Power Systems
DAQ	Data Acquisition
ESRDC	Electric Ship Research and Development Consortium
HIL	Hardware in the Loop
IPS	Integrated Power System
KE	Kinetic Energy
LTI	Linear Time-Invariant
MVAC	Medium Voltage Alternating Current
MVDC	Medium Voltage Direct Current
NI	National Instruments
NTC	Negative Temperature Coefficient
NGIPS	Next Generation Integrated Power System
ONR	Office of Naval Research
PE	Potential Energy
PCM	Power Conversion Module
PGM	Power Generation Module
RTDS	Real Time Digital Simulator
SSCM	Ship Service Converter Module
SSIM	Ship Service Inverter Module
USN	United States Navy
USA	United States of America

B Mathematica Code

<< ToMatlab`

Rearrange Equations

lse = Solve[

$\Big\{$Tx2o == Tx2i $-\frac{\text{mx1}*\text{cpsw}}{\text{mx2}*\text{cpfw}} * (\text{Tx1o} - \text{Tx1i})$,

ex == $\frac{\text{mx1}*\text{cpsw}*(\text{Tx1o}-\text{Tx1i})}{\text{mx2}*\text{cpfw}*(\text{Tx2i}-\text{Tx1i})}$,

Tx2i == $\frac{\text{m1}*\text{T1o}+\text{m2}*\text{T2o}+\text{m3}*\text{T3o}}{\text{m1}+\text{m2}+\text{m3}}$,

T1o == e1 $*$ T1 $+ (1 -$ e1$) *$ Tx2o,

T2o == e2 $*$ T2 $+ (1 -$ e2$) *$ Tx2o,

T3o == e3 $*$ T3 $+ (1 -$ e3$) *$ Tx2o$\}$, $\{$T1o, T2o, T3o, Tx1o, Tx2i, Tx2o$\}$];

$\{$T1o, T2o, T3o, Tx1o, Tx2i, Tx2o$\}$ = $\{$T1o, T2o, T3o, Tx1o, Tx2i, Tx2o$\}$/.Flatten[lse];

T1o = FullSimplify[T1o];

T2o = FullSimplify[T2o];

T3o = FullSimplify[T3o];

Tx1o = FullSimplify[Tx1o];

Tx2i = FullSimplify[Tx2i];

Tx2o = FullSimplify[Tx2o];

T1D = FullSimplify $\left[\frac{1}{\text{M1}*\text{c1}} * (\text{Q1} + 31 * \text{A1} * (\text{Tamb} - \text{T1}) + \text{m1} * \text{cpfw}(\text{Tx2o} - \text{T1o}))\right]$;

T2D = FullSimplify $\left[\frac{1}{\text{M2}*\text{c2}} * (\text{Q2} + 32 * \text{A2} * (\text{Tamb} - \text{T2}) + \text{m2} * \text{cpfw}(\text{Tx2o} - \text{T2o}))\right]$;

T3D = FullSimplify $\left[\frac{1}{\text{M3}*\text{c3}} * (\text{Q3} + 33 * \text{A3} * (\text{Tamb} - \text{T3}) + \text{m3} * \text{cpfw}(\text{Tx2o} - \text{T3o}))\right]$;

Find Coefficients

System Matrix Entries (A Matrix)

T1DcoeffT1 = FullSimplify[Coefficient[T1D, T1]];

T1DcoeffT2 = FullSimplify[Coefficient[T1D, T2]];

T1DcoeffT3 = FullSimplify[Coefficient[T1D, T3]];

T2DcoeffT1 = FullSimplify[Coefficient[T2D, T1]];

T2DcoeffT2 = FullSimplify[Coefficient[T2D, T2]];

T2DcoeffT3 = FullSimplify[Coefficient[T2D, T3]];

T3DcoeffT1 = FullSimplify[Coefficient[T3D, T1]];

T3DcoeffT2 = FullSimplify[Coefficient[T3D, T2]];

T3DcoeffT3 = FullSimplify[Coefficient[T3D, T3]];

Input Matrix Entries (B Matrix)

T1DcoeffQ1 = FullSimplify[Coefficient[T1D, Q1]];

T1DcoeffQ2 = FullSimplify[Coefficient[T1D, Q2]];

T1DcoeffQ3 = FullSimplify[Coefficient[T1D, Q3]];

T2DcoeffQ1 = FullSimplify[Coefficient[T2D, Q1]];

T2DcoeffQ2 = FullSimplify[Coefficient[T2D, Q2]];

T2DcoeffQ3 = FullSimplify[Coefficient[T2D, Q3]];

T3DcoeffQ1 = FullSimplify[Coefficient[T3D, Q1]];

T3DcoeffQ2 = FullSimplify[Coefficient[T3D, Q2]];

T3DcoeffQ3 = FullSimplify[Coefficient[T3D, Q3]];

Output Matrix Entries (C Matrix)

```
T1ocoeffT1 = FullSimplify[Coefficient[T1o, T1]];
T1ocoeffT2 = FullSimplify[Coefficient[T1o, T2]];
T1ocoeffT3 = FullSimplify[Coefficient[T1o, T3]];
T2ocoeffT1 = FullSimplify[Coefficient[T2o, T1]];
T2ocoeffT2 = FullSimplify[Coefficient[T2o, T2]];
T2ocoeffT3 = FullSimplify[Coefficient[T2o, T3]];
T3ocoeffT1 = FullSimplify[Coefficient[T3o, T1]];
T3ocoeffT2 = FullSimplify[Coefficient[T3o, T2]];
T3ocoeffT3 = FullSimplify[Coefficient[T3o, T3]];
Tx1ocoeffT1 = FullSimplify[Coefficient[Tx1o, T1]];
Tx1ocoeffT2 = FullSimplify[Coefficient[Tx1o, T2]];
Tx1ocoeffT3 = FullSimplify[Coefficient[Tx1o, T3]];
Tx2icoeffT1 = FullSimplify[Coefficient[Tx2i, T1]];
Tx2icoeffT2 = FullSimplify[Coefficient[Tx2i, T2]];
Tx2icoeffT3 = FullSimplify[Coefficient[Tx2i, T3]];
Tx2ocoeffT1 = FullSimplify[Coefficient[Tx2o, T1]];
Tx2ocoeffT2 = FullSimplify[Coefficient[Tx2o, T2]];
Tx2ocoeffT3 = FullSimplify[Coefficient[Tx2o, T3]];
```

D Matrix Entries

```
T1ocoeffQ1 = FullSimplify[Coefficient[T1o, Q1]];
T1ocoeffQ2 = FullSimplify[Coefficient[T1o, Q2]];
T1ocoeffQ3 = FullSimplify[Coefficient[T1o, Q3]];
```

```
T2ocoeffQ1 = FullSimplify[Coefficient[T2o, Q1]];
T2ocoeffQ2 = FullSimplify[Coefficient[T2o, Q2]];
T2ocoeffQ3 = FullSimplify[Coefficient[T2o, Q3]];
T3ocoeffQ1 = FullSimplify[Coefficient[T3o, Q1]];
T3ocoeffQ2 = FullSimplify[Coefficient[T3o, Q2]];
T3ocoeffQ3 = FullSimplify[Coefficient[T3o, Q3]];
Tx1ocoeffQ1 = FullSimplify[Coefficient[Tx1o, Q1]];
Tx1ocoeffQ2 = FullSimplify[Coefficient[Tx1o, Q2]];
Tx1ocoeffQ3 = FullSimplify[Coefficient[Tx1o, Q3]];
Tx2icoeffQ1 = FullSimplify[Coefficient[Tx2i, Q1]];
Tx2icoeffQ2 = FullSimplify[Coefficient[Tx2i, Q2]];
Tx2icoeffQ3 = FullSimplify[Coefficient[Tx2i, Q3]];
Tx2ocoeffQ1 = FullSimplify[Coefficient[Tx2o, Q1]];
Tx2ocoeffQ2 = FullSimplify[Coefficient[Tx2o, Q2]];
Tx2ocoeffQ3 = FullSimplify[Coefficient[Tx2o, Q3]];

D1 = {{T1ocoeffQ1, T1ocoeffQ2, T1ocoeffQ3},
{T2ocoeffQ1, T2ocoeffQ2, T2ocoeffQ3},
{T3ocoeffQ1, T3ocoeffQ2, T3ocoeffQ3},
{Tx1ocoeffQ1, Tx1ocoeffQ2, Tx1ocoeffQ3},
{Tx2icoeffQ1, Tx2icoeffQ2, Tx2icoeffQ3},
{Tx2ocoeffQ1, Tx2ocoeffQ2, Tx2ocoeffQ3}};
```

Offset

```
OffT1D = FullSimplify[T1D − (T1 ∗ T1DcoeffT1 + T2 ∗ T1DcoeffT2 + T3
∗T1DcoeffT3 + Q1 ∗ T1DcoeffQ1 + Q2 ∗ T1DcoeffQ2 + Q3 ∗ T1DcoeffQ3)];
```

OffT2D = FullSimplify[T2D − (T1 ∗ T2DcoeffT1 + T2 ∗ T2DcoeffT2 + T3
∗T2DcoeffT3 + Q1 ∗ T2DcoeffQ1 + Q2 ∗ T2DcoeffQ2 + Q3 ∗ T2DcoeffQ3)];
OffT3D = FullSimplify[T3D − (T1 ∗ T3DcoeffT1 + T2 ∗ T3DcoeffT2 + T3
∗T3DcoeffT3 + Q1 ∗ T3DcoeffQ1 + Q2 ∗ T3DcoeffQ2 + Q3 ∗ T3DcoeffQ3)];

OffsetAB = {{OffT1D}, {OffT2D}, {OffT3D}};

OffT1o = FullSimplify[T1o − (T1 ∗ T1ocoeffT1 + T2 ∗ T1ocoeffT2 + T3
∗T1ocoeffT3 + Q1 ∗ T1ocoeffQ1 + Q2 ∗ T1ocoeffQ2 + Q3 ∗ T1ocoeffQ3)];
OffT2o = FullSimplify[T2o − (T1 ∗ T2ocoeffT1 + T2 ∗ T2ocoeffT2 + T3
∗T2ocoeffT3 + Q1 ∗ T2ocoeffQ1 + Q2 ∗ T2ocoeffQ2 + Q3 ∗ T2ocoeffQ3)];
OffT3o = FullSimplify[T3o − (T1 ∗ T3ocoeffT1 + T2 ∗ T3ocoeffT2 + T3
∗T3ocoeffT3 + Q1 ∗ T3ocoeffQ1 + Q2 ∗ T3ocoeffQ2 + Q3 ∗ T3ocoeffQ3)];
OffTx1o = FullSimplify[Tx1o − (T1 ∗ Tx1ocoeffT1 + T2 ∗ Tx1ocoeffT2 + T3
∗Tx1ocoeffT3 + Q1 ∗ Tx1ocoeffQ1 + Q2 ∗ Tx1ocoeffQ2 + Q3 ∗ Tx1ocoeffQ3)];
OffTx2i = FullSimplify[Tx2i − (T1 ∗ Tx2icoeffT1 + T2 ∗ Tx2icoeffT2 + T3
∗Tx2icoeffT3 + Q1 ∗ Tx2icoeffQ1 + Q2 ∗ Tx2icoeffQ2 + Q3 ∗ Tx2icoeffQ3)];
OffTx2o = FullSimplify[Tx2o − (T1 ∗ Tx2ocoeffT1 + T2 ∗ Tx2ocoeffT2 + T3
∗Tx2ocoeffT3 + Q1 ∗ Tx2ocoeffQ1 + Q2 ∗ Tx2ocoeffQ2 + Q3 ∗ Tx2ocoeffQ3)];

OffsetCD = {{OffT1o}, {OffT2o}, {OffT3o}, {OffTx1o}, {OffTx2i}, {OffTx2o}};

Convert To Matlab

ToMatlab[A];

ToMatlab[B];

ToMatlab[C1];

```
ToMatlab[D1];

ToMatlab[OffsetAB];

ToMatlab[OffsetCD];
```

C Simulation Parameters

Parameter	Comment	Value	Unit
$\dot{m}_1$	Mass flow rate of deionized water through device 1.	0,1	$\frac{kg}{s}$
$\dot{m}_2$	Mass flow rate of deionized water through device 2.	0,02	$\frac{kg}{s}$
$\dot{m}_3$	Mass flow rate of deionized water through device 3.	0,07886	$\frac{kg}{s}$
$\dot{m}_{x1}$	Mass flow rate of seawater through primary cooling cycle.	0,5	$\frac{kg}{s}$
c_{pfw}	Specific heat of deionized water at constant pressure.	4183	$\frac{J}{kg\,K}$
c_{psw}	Specific heat of seawater at constant pressure.	3993,7	$\frac{J}{kg\,K}$
ε_1	Heat exchanger effectiveness between device 1 and cooling water.	0,9	
ε_2	Heat exchanger effectiveness between device 2 and cooling water.	0,9	
ε_3	Heat exchanger effectiveness between device 3 and cooling water.	0,9	
ε_x	Heat exchanger effectiveness between primary and secondary cooling cycle.	0,9	
M_1	Mass of device 1.	15	kg
M_2	Mass of device 2.	6	kg
M_3	Mass of device 3.	3	kg
A_1	Outer surface area of device 1.	0,8	m^2
A_2	Outer surface area of device 2.	0,5	m^2
A_3	Outer surface area of device 3.	0,3	m^2
h_1	Convection heat transfer coefficient between device 1 and atmosphere.	10	$\frac{W}{m^2\,K}$
h_2	Convection heat transfer coefficient between device 2 and atmosphere.	10	$\frac{W}{m^2\,K}$
h_3	Convection heat transfer coefficient between device 3 and atmosphere.	10	$\frac{W}{m^2\,K}$
c_1	Specific heat of device 1.	435	$\frac{J}{kg\,K}$
c_2	Specific heat of device 2.	435	$\frac{J}{kg\,K}$
c_3	Specific heat of device 3.	435	$\frac{J}{kg\,K}$

Table 2: Simulation parameters.

Parameter	Comment	Value	Unit
$\dot{Q}_1$	Power dissipated by device 1.	4000	W
$\dot{Q}_2$	Power dissipated by device 2.	1000	W
$\dot{Q}_3$	Power dissipated by device 3.	1500	W
T_{amb}	Ambient temperature.	20	°C
T_{x1i}	Temperature at the water inlet of the primary side of the heat exchanger, between primary and secondary cooling cycle.	20	°C

Table 3: Simulation parameters.